GOLD NANOPARTICLE DIMERS FOR SERS-BASED TARGETED DETECTION OF HUMAN GLIOBLASTOMA CELLS

by

BRYAN PALADINI

A thesis submitted to the

Graduate School- New Brunswick

Rutgers, The State University of New Jersey

In partial fulfillment of the requirements

For the degree of

Master of Science

Graduate Program in

Materials Science and Engineering

Written under the direction of

Professor Laura Fabris

And approved by

_____

_____

_____

New Brunswick, New Jersey

OCTOBER 2011

ABSTRACT OF THE THESIS

Gold Nanoparticle Dimers for SERS-Based Targeted Detection of Human Glioblastoma Cells

By BRYAN PALADINI

Thesis Director:

Dr. Laura Fabris

Gold nanospheres are linked by a Raman active dithiolated linker molecule forming dimer and trimer assemblies. These nanoparticles are capped with polyethylene glycol for stability and functionalized with peptides for glioblastoma cell targeting and penetration. Results show stability *in vitro* and cellular uptake of the nanoparticles. After endocytosis, a surface enhanced Raman scattering signal from the nanoparticles can be detected from inside the cells. Such a nanoparticle systems sets the ground work for developing versatile Raman-based tools designed for a range of biomedical applications.

ACKNOWLEDGEMENTS

I would like to thank Dr. Laura Fabris, Paul Mark and Robert Wadams of the Rutgers Materials Science and Engineering Department for their support and assistance in developing this thesis. I would also like to thank Dr. Prabhas Moghe, Dr. Charles Roth, Dominik Naczynski, and Joseph Kim of the Rutgers Biomedical Engineering Department for their instruction and guidance in cell culture and fluorescent microcopy, and for providing the U87 cells used in this work.

TABLE OF CONTENTS

LIST OF TABLES

LIST OF FIGURES

1. INTRODUCTION

Cancer is a lethal disease responsible for hundreds of thousands of deaths each year in the United States alone [1]. Of the many types of cancer, glioblastoma is arguably one of the most deadly. The life expectancy after diagnosis is typically only one year [2]. Researchers must strive to develop new therapeutic methods to combat this life-threatening disease.

Unfortunately, therapeutics against brain cancer are somewhat limited due to the presence of the blood brain barrier [3], a contiguous layer of endothelial cells circumferentially surrounding the cell margin at the brain capillaries. This barrier restricts the transfer of hydrophilic compounds, small proteins and charged molecules from the blood plasma to the central nervous system. It also creates difficulties in the delivery of biomarkers and therapeutic drugs. However, biomaterials on the nanometer scale (<100 nm) have shown the ability to partially cross this barrier. Researchers have developed nanoparticles that have successfully crossed the blood brain barrier *in vivo* [4]. A nanoparticle-based system small enough to cross the barrier and target specific cells would be an invaluable diagnostic tool in the fight against brain cancer.

Researchers are beginning to incorporate Raman active molecules into the synthesis of nanoparticle systems as a novel optical detection method. These types of molecules have distinct Raman spectra characterized by narrow peaks and specific peak patterns. The Raman signals of molecules adsorbed or linked to the surface of noble metal nanoparticles can be significantly enhanced owing to the surface enhanced Raman scattering effect. Arranging the

nanoparticles in a dimer configuration exploits the strong electromagnetic field in between the junctions of the metal nanoparticles leading to an even higher signal enhancement. Functionalization of these metallic dimers with stabilizing polymers and targeting moieties leads to decreased fouling and increased selective uptake. The use of such systems for cell targeting of glioblastoma cells *in vitro* with subsequent Raman signal detection sets the ground work for developing future *in vivo* Raman-based diagnostic tools.

2. BACKGROUND

2.1. Biomedicine and Nanotechnology

The field of nanoscience has expanded significantly over these last few decades. The ability to create, functionalize, and characterize particles with sizes in the range between 1 and 100 nm has allowed researchers to better understand the capabilities this field has to offer. Most recently the incorporation of nano-sized technology in biomedicine has shown significant progress in the field of therapeutics [5-8].

In the fight against glioblastoma, patients are treated with chemotherapy and radiology in addition to surgery [2]. To avoid the side effects of chemotherapy and radiotherapy, researchers are developing methods to specifically target cancerous cells. There are known physical differences between healthy cells and different types of cancerous cells, such as integrin expression, that can be exploited for targeting purposes [9]. Treating only targeted cancerous cells with drug molecules will avoid the side effect of killing healthy cells. In addition, the ability to deliver nanoparticle systems to specific targeted cells can provide important diagnostic and imaging information.

There are many nanomaterials that have been designed for biomedical applications. For example, researchers have the capability to create nano-sized liposomes [10], dendrimers [11] and polymeric particles [12]. These nanoparticles have subsequently been used for cell targeting [13], imaging [14], detection [15], and drug delivery [16] applications. A common technique for

tracking these particles is to label them with fluorescent molecules. However, these dyes are subject to an effect called photobleaching. After a period of continuous fluorescence, the chemistry of the molecule irreversibly changes and the amount of emitted photons decays down to zero [17]. To override this issue, researchers have incorporated an alternative method for optical detection: metallic nanoparticles.

2.2. Metallic Nanoparticles for Biomedicine

Metallic nanoparticles have been around long before modern advances in nanotechnology. For millennia, gold nanoparticles have been used for their distinct, decorative red color. In ancient times, nanoparticles were suspended in glasses to create ruby red colors [18]. In the renaissance, nanoparticles were incorporated in the decoration of pottery art [19]. It wasn't until the 19th century however, when Michael Faraday first studied these gold nanoparticle colloids, that the science behind the optics came to light [20]. Today, the study and use of colloidal metals has reached new heights with the exploration of new applications for their optical properties. The quantum scale dimensions of these nano-sized metallic particles have shown to impart unique and tunable properties that can be designed to specifically target various applications. For these reasons, researchers are incorporating nano-sized metallic structures in the design of nanosized biosensing, bioimaging, and drug delivery systems [21]. These structures can be designed based on shape, size, and material. In this work, gold nanospheres in the range of 20 to 30 nm are used.

2.3. Metallic Nanoparticle Synthesis

Gold nanoparticles can be synthesized to possess many different shapes, such as rods [22], stars [23], or cubes [24]. However, the simplest nanoparticle is the sphere. The traditional method developed by Turkevich, et *al*. involves the formation of gold nanospheres via the addition of trisodium citrate to a heated aqueous solution of tetrachloroauric acid [25]. This is a multiple step process [26]:

The $HAuCl_4$ salt disproportionates when added to water:

$$HAuCl_4 \rightarrow AuCl_3 + H^+ + Cl^-$$

The oxidation of citrate yields dicarboxy acetone:

$$C_3H_5O(COO)_3^{3-} \rightarrow C_3H_4O(COO)_2^{2-} + CO_2 + H^+ + 2e^-$$

Followed by the reduction of auric salt to aurous salt:

$$AuCl_3 + 2e^- \rightarrow AuCl + 2Cl^-$$

Then, the disproportionation of aurous species to aurous salt:

$$3AuCl \rightarrow 2Au^0 + AuCl_3$$

Meanwhile, the dicarboxy acetone forms acetone:

$$2H_2O + C_3H_4O(COO)_2^{2-} \rightarrow (CH_3)_2C{=}O + 2CO_2 + 2(OH)^-$$

Acetone will reduce the auric salt that in turn leads to the formation of gold atoms, Au^0, during disproportionation.

Once nucleation of the gold particles occurs, the adsorption of the gold atoms, Au^0, will cause the particle to grow in size. The nanosized particles are then capped with a monolayer of the remaining citrate molecules. This

monolayer provides a negative charge on the surface of the spheres. The stability of the particles arises from the positively charged counterion cloud surrounding the surface. This counterion cloud provides the repelling force that counteracts aggregation. It is this electrostatic stability that allows the gold nanospheres to be suspended in a colloidal solution. However, the formation of gold nanospheres is not necessarily limited to a citrate reduction synthesis. For example, Brust, et *al*. developed a method for the synthesis of dodecanethiol stabilized gold nanoparticles using a two-phase system [27].

2.4. Optical Properties of Metallic Nanoparticles

2.4.1. Surface Plasmon Resonance

As incident photons approach a metallic surface or particle, the oscillating electromagnetic field will cause a coherent oscillation of the conduction electrons. This was first discovered by Gustav Mie in 1908 [28]. The oscillating shift of the electron cloud is balanced by the Coulomb attractive force between the electrons and the nuclei in the nanoparticle lattice (fig. 1).

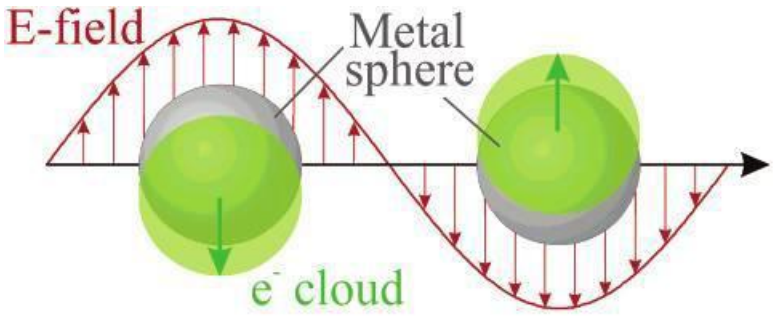

Figure 1: Schematic of plasmon oscillation for a sphere [29].

Such an oscillation is called the dipole plasmon resonance. The frequency of the plasmon is dependent on the density of electrons, the effective electron mass, and the size and shape of the charge distribution. The oscillation that occurs at the surface is referred to as the Surface Plasmon Resonance (SPR) [30].

The polarizability of the SPR is related to the dielectric constant of the surrounding medium (ε_m), the volume of the nanoparticle (V), and the dielectric constant of the metal (ε), which is dependent on the frequency of the incident photons.

$$\alpha = 3\varepsilon_0 V \frac{(\varepsilon - \varepsilon_m)}{(\varepsilon + 2\varepsilon_m)}$$

Where ε_0 is the vacuum permittivity. As can be seen in the equation, the polarizability is at a maximum where ε is roughly equal to $-2\varepsilon_m$. For metallic particles, this ε occurs at frequencies in the visible range. The SPR at this frequency causes a large local electric field enhancement along with strong light absorption and scattering properties.

In instances of a metallic nanosphere where the radius is much smaller than the wavelength of the incident light, the extinction cross-section can be calculated using the Mie Theory [30].

$$C_{ext} = \frac{24\pi^2 R^3 \varepsilon_m^{3/2}}{\lambda} \frac{\varepsilon_i}{(\varepsilon_r + 2\varepsilon_i)^2 + 2\varepsilon_i^2}$$

Therefore a maximum adsorption peak can occur when the real part of the extinction coefficent (ε_r) is roughly equal to $-2(\varepsilon_m)$ and the imaginary part of

the extinction coefficent (ε_i) is low. This is observed when characterizing metallic nanoparticles with photospectroscopy that relates the absorbance to the wavelength of the incident electromagnetic energy. Any changes to the dielectric constant of the surrounding medium (ε_m) or nanosphere size (R) will cause the absorption peak to shift (fig. 2) [30].

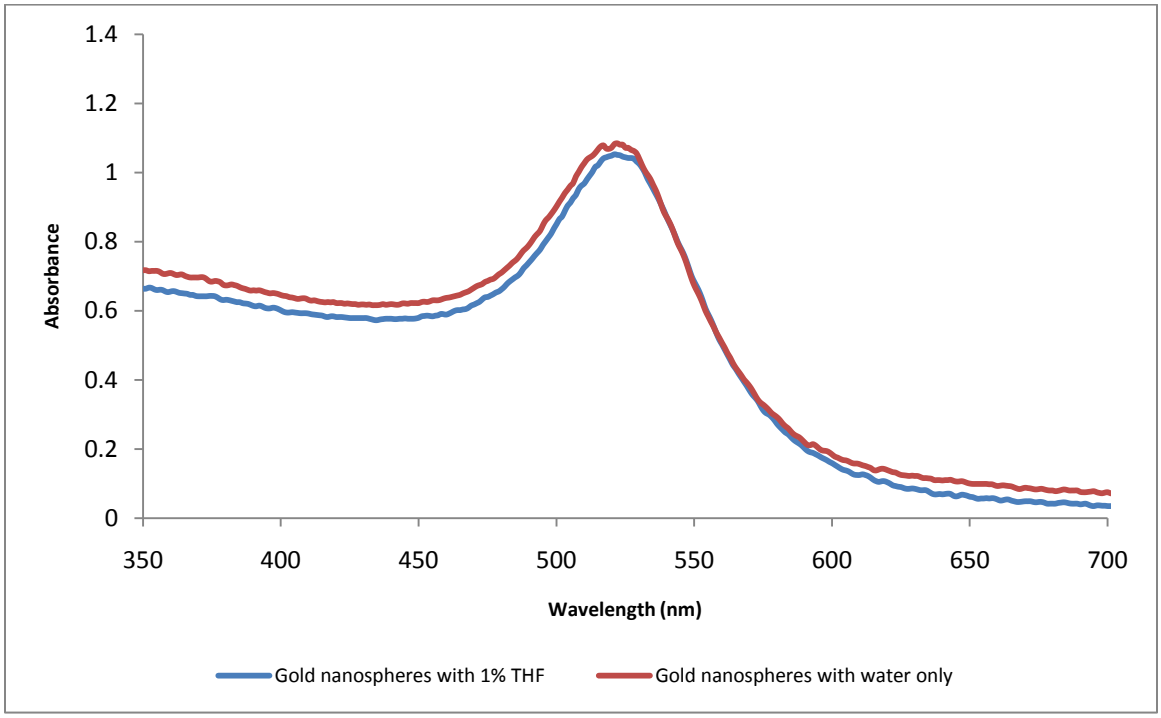

Figure 2: Example of a plasmon shift due to a change in the surrounding medium.

The Beer-Lambert Law tells us that the concentration of an absorbing species (C) is related to the absorbance of a monochromatic light (A), its path length in the absorbing medium (l), and the extinction coefficient of the absorbing species (ε) [31].

$$C = \frac{A}{(\varepsilon \times l)}$$

Metallic nanoparticles have a SPR peak at specific wavelengths and its absorbance can be measured with a spectrophotometer. The path length (l) will vary based on the particular spectrophotometer used and once the extinction coefficient (ε) is known, the concentration (C) for a particular colloidal system can be determined. Research has shown that the extinction coefficient for a gold nanoparticle can be calculated based on size, shape and composition [32, 33]. Information on the particular size and shape of a gold colloidal suspension can be determined using transmission electron microscopy (TEM). Xiong Liu, et. *al.* used high resolution transmission electron microscopy analysis and UV–vis absorption spectroscopy measurements to develop an equation that relates the size of citrate capped gold nanospheres suspended in water with an equivalent extinction coefficient [34].

$$\ln \varepsilon = k \ \ln D + a$$

Where (ε) is the extinction coefficient, (D) is the diameter of the gold nanoparticle and (k) and (a) are constants calculated to be 3.32111 and 10.80505, respectively. With this information, the concentration of a colloidal suspension of gold nanospheres can be determined using spectrophotometry once the size of the particles is known.

The SPR scattering effect can be utilized in optical detection. Because of maximum scattering in the optical region, biomaterials that incorporate metallic nanoparticles can be used as biosensors. For example, El-Sayed, et. *al.* were able to conjugate an anti-growth factor receptor onto the surface of a gold nanoparticle allowing it to cross the cell membrane of HeLa cells [35]. Light

scattering imagery was then used to image the cells. The SPR scattering of the nanoparticles was able to cause an observable color that indicated the location of the cancerous cells.

Additionally, the interaction of nanoparticles in close proximity to each other can affect the SPR properties. As two or more nanoparticles approach each other, the SPR of each can couple together causing a red shift in the peak wavelength. This is called plasmon coupling. This can be useful in determining if the nanoparticles are beginning to flocculate. This phenomenon was exploited by Mirkin, et *al.* in detecting single DNA molecules [36]. In that approach, thiolated ssDNA was adsorbed onto gold nanospheres. When ssDNA complementary to the already adsorbed strands, was introduced in the suspension, hybridization occurred causing the particles to assemble. The reduction in the inter-particle distance caused a red shift in the SPR as observed by a color transition from red to purple.

The optical advantages of metallic nanoparticles are not limited to the absorption and scattering properties of SPR. In addition, the large local electric field created by the SPR can be used to drastically increase the Raman signal of a small molecule. This increase is significant enough to be used as a marker in biosensing.

2.4.2. Fluorescence and Raman Scattering

The interaction of light and the energy states of a molecule provides important information about the properties of a material. As a molecule absorbs

an incident photon it will transition from a lower energy state to a higher energy state. Rayleigh elastic scattering is said to occur when the molecule relaxes to the initial energy state and emits a photon with the same wavelength as the incident photon. However, if there is a shift from the wavelength of the initial absorbed photon to a different wavelength for the emitted photon, the scattering is considered inelastic [17].

As light is irradiated on a molecule, absorption of a photon will excite an electron from the fundamental singlet state, S_0, to an excited singlet state, S_1. Over a finite period of time, the electron can relax down to a vibrational sub-structure of S_1 via internal conversion (IC). This electron can then transition back down to S_0, which causes the emission of a photon. Because of the IC, the emitted photon is at a different energy then the absorbed photon. This phenomenon is called fluorescence. Certain molecules, such as Fluorescein Isothiocyanate (FITC), are well known for their fluorescent properties in the optical region. A fluorescence microscope allows a user to excite a molecule at a specific excitation wavelength using a laser beam and to optically observe only the resultant fluorescence by filtering out all but the emission wavelength.

Raman scattering is a well known inelastic scattering effect first discovered by Chandrasekhara Raman in 1922 [37]. As the incident photon is absorbed, an electron in the fundamental singlet state S_0 transitions to a virtual energy state instead of an excited singlet state S_1. Simultaneously, the molecule relaxes back to S_0 but at a different vibrational energy. This vibrational energy can be a higher state (Stokes) or a lower state (anti-Stokes) than the initial

energy state. The energy difference consequently causes the emission photon to be at a different wavelength then the absorbed photon. In cases where the virtual state coincides with a real electronic state of the molecule, resonant scattering occurs. This can cause the scattering intensity to increase by several orders of magnitude [17].

Molecules that have multiple vibrational modes will have varying degrees of wavelength shift. As a result, the intensity of the emitted photons can be plotted against the excitation wavelength shift.

The Raman peak pattern is unique to the irradiated molecule. Because of this, certain highly Raman active molecules can be useful for labeling, such as for example biphenyl-4,4’-dithiol (DBDT, fig. 3). A disadvantage of Raman is the low intensity of the spectra. Fortunately, an effect called surface enhanced Raman scattering, that arises in the presence of noble metal nanoparticles or rough metallic surfaces, allows the signal to be increased by several orders of magnitude.

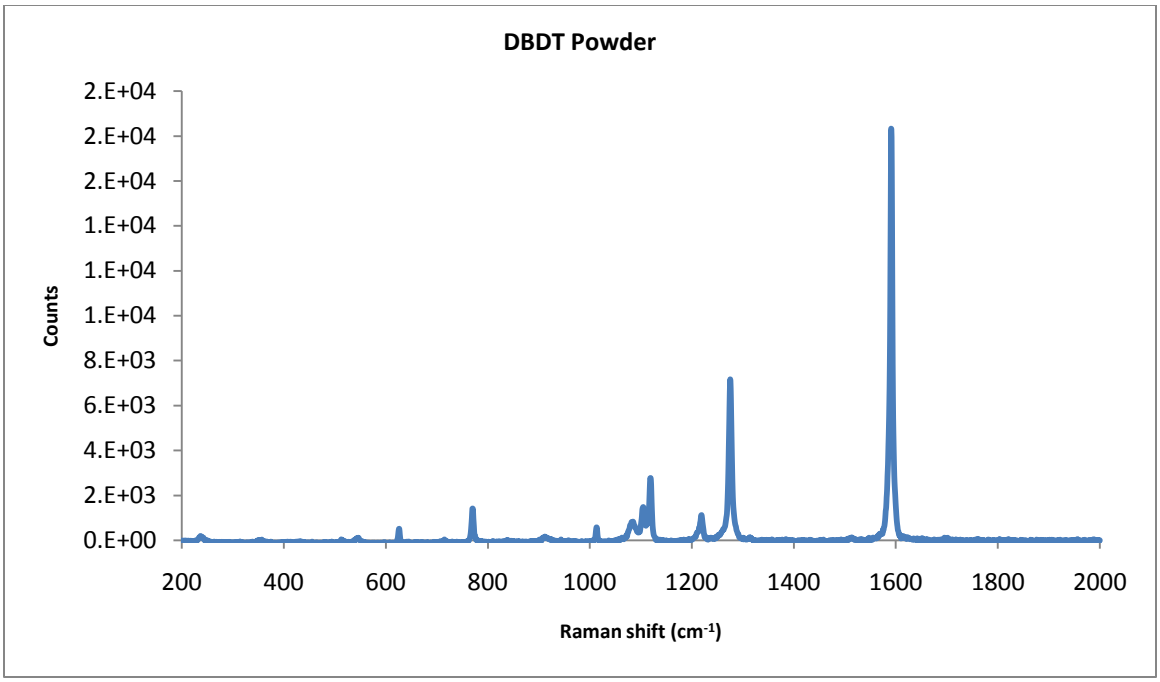

Figure 3: Raman spectra of biphenyl-4,4'-dithiol (DBDT)

2.4.3. Surface Enhanced Raman Scattering (SERS)

The SERS effect was first discovered by Fleischmann et *al*. in 1974 [38]. Scientists soon realized that an amplification of a Raman signal can occur due to an electromagnetic interaction between the laser light and metal structures with sizes smaller than the laser wavelength. This amplification can be of several orders of magnitude.

As discussed before, light irradiated on a metal can generate surface plasmons. The irradiance of a nanoparticle or a surface with nanoscale roughness can create surface plasmon resonances. These plasmons create large local field enhancements that affect molecules adsorbed, bound, or in close proximity to the nanoparticle surface. The normal Raman scattering of the

molecule is enhanced by two factors; an electromagnetic enhancement and a chemical enhancement.

The electromagnetic enhancement is due to the increase in the electromagnetic field strength at the surface caused by the excitation of surface plasmons resonances. A coupling of the incident electromagnetic field and the resultant Raman electromagnetic field leads to an increase in the output Raman signal. The degree of this increase depends greatly on the proximity of the molecule to the metallic surface. A separation of more than a few nanometers will lead to a drastic decrease of the enhancement.

A separate chemical enhancement, based on the charge transfer theory, arises from the modification of the electronic polarizability of the Raman molecule inducing resonant-Raman scattering at wavelengths where the molecule would otherwise not be resonant [39]. A molecule in resonance with the incident electromagnetic field will lead to a higher Raman signal than a non-resonant one. However, for this to occur, the molecule must be adsorbed to the surface of the metallic nanoparticle. While this enhancement increases the Raman signal, the degree that it does so is much less then the electromagnetic enhancement. The combination of these two enhancements can create signal increases of 10^5 to 10^6 [17].

2.4.4. SERS of Metallic Nanoparticle Dimers

When applied under optimal conditions, such as single molecules located at areas of strongly localized electromagnetic fields, and at an excitation

frequency resonant with the metallic particle's SPR, a SERS enhancement can be as high as 10^{10} to 10^{11} [17]. Xu, et *al.* adsorbed hemoglobin molecules on the surface of silver nanoparticles [40]. Because hemoglobin can adsorb to more than one particle at a time, some of the nanoparticle monomers were able to assemble into dimers and trimers in the presence of the protein. The concentration of hemoglobin was kept low to ensure that only a few molecules would adsorb to each nanoparticle. Such a condition allowed for single molecule detection as individual molecules adsorbed to specific hot spots of high enhancement. The solution was scanned with a Raman spectrometer at an excitation wavelength close to a SPR of the nanocluster. Results showed an enhancement factor of approximately 2.5×10^{10}. Further studies using atomic force microscopy (AFM) showed that the highest enhancements originated from the hemoglobin molecules in between the junctions of the dimers and trimers particles. None of the monomers observed had the same intensity as the dimers and trimers. Additionally, the degree of enhancement from the dimers and trimers was highly dependent on the inter-particle distance in the junctions. As the distance increased from 1 nm in the single molecule condition to 5.5 nm in a solution supersaturated with hemoglobin, the enhancement factor dropped down to approximately 6×10^{6}. The highly localized electric field between the dimers and trimers is what lead to the high Raman signal enhancements.

As discussed before, plasmon coupling from aggregation can cause a shift in a particle's SPR. This is also true when monomers are formed into dimers. Studies of gold nanoparticle dimers have shown an ability of the SPR to be

modified based on the inter-particle distance between the particles. As the distance decreases, a red shift of the SPR occurs [41].

In biology, a common method for detection is the use of fluorescent dyes that can provide an optical signal when excited with a laser. However, nanoparticles that take advantage of SERS by incorporating Raman molecules have some distinct advantages over fluorophores: namely a lack of photobleaching and the ability for multiplexing.

Over time, as a fluorophore is continuously excited, the degree of fluorescence decays. This is a consequence related to the molecular excitation. When an electron is excited to a singlet state there is a probability that the electron will transition to a triplet state via intersystem crossing (ISC), leading to phosphorescence, instead of relaxing to the ground state. The high chemical reactivity of the triplet state can lead to irreversible changes in the molecules structure preventing any further fluorescence. The probability of ISC is low, leading to low photobleaching rates, however over time a continuously irradiated fluorescent molecule can irreversibly change structure and lose fluorescence intensity. On the other hand, Raman molecules, also known as Raman reporters, do not change their structure as they only reach a virtual state when excited [17]. Therefore, the signal obtained from a Raman reporter will not decay over time.

When plotting the emission spectra of a fluorophore versus wavelength, broad peaks are observed. When multiple fluorophores are plotted on the same graph, overlapping begins to occur. If a large number of fluorophores are added

to a system there is a possibility that optical separation may be impossible as multiple fluorophores can be excited with the same frequency. Therefore, in biodetection, the number of usable fluorophores at any one time is limited. However, due to the distinct spectra obtained from Raman reporters, there is less risk of overlap. Multiple Raman reporters added to a system can be separated based on the specific SERS peaks that are unique to each molecule. Multiplexing of Raman reporters on gold nanoparticles can be accomplished by systematic additions of varying thiolated molecules [42]. The wide variation in Raman reporters leads to an almost infinite number of permutations for labeling particles. Essentially, Raman reporters can be used to tag nanoparticle systems for any number of applications.

The Raman reporter used for this work is the DBDT molecule discussed before. It is a small molecule consisting of two connected benzene rings with thiol functional groups on each end (fig 4).

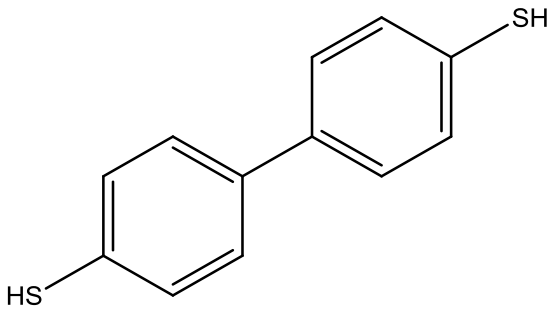

Figure 4: Chemical structure of DBDT.

Using X-ray photoelectronspectroscopy (XPS), the length of DBDT was estimated to be 1.65 ± 0.125 nm [43]. The small length ensures that the dimers form inter-particle distances in the range necessary to achieve high SERS

enhancements. In characterizing the absorption spectra of DBDT and similar dithiols, Boer, et *al*. used tetrahydrofuran (THF) as a solvent [44].

2.5. Nanoparticle Stability

In developing a nanoparticle colloidal system, emphasis needs to be placed on the stability of the system. If aggregation occurs, the properties of the system can change and this may defeat the purpose of the system. In metallic nanoparticle systems, the surfactants provide the source of stability.

The binding affinity of the ligands determines preference for adsorption. A ligand with a higher binding coefficent will replace a ligand with a lower one. Because of this, gold nanoparticles can be functionalized with specific ligands depending on the sequence of additions. For example, bis(p-sulfonatophenyl)phenylphosphine dihydrate dipotassium salt (BSPP) is a phosphine ligand which has a binding affinity for gold higher than citrate but lower than thiols (fig. 5). A ligand exchange can create a stronger negative charge on the gold surface which will increase the stability of the particles. This ligand has been used by researchers as a strongly negatively charged, intermediate surfactant between a citrate synthesized gold nanospheres and gold nanospheres functionalized with a ssDNA monolayer [45].

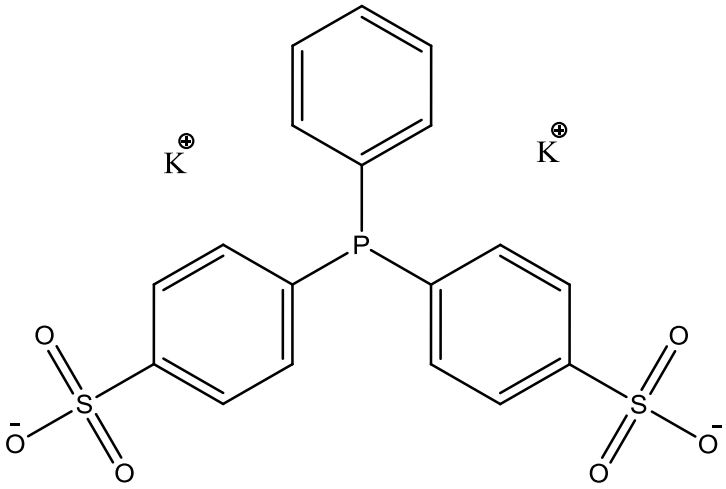

Figure 5: Chemical structure of BSPP.

As discussed before, citrate-capped gold nanospheres are stabilized by electrostatic charges. As a result, flocculation is dependent on the ionic strength of the suspension [46]. Additionally, studies have shown that proteins in human blood can adsorb to the surface of citrate-capped gold nanoparticles [47]. This can lead to aggregation under certain conditions. Depending on the application of the nanoparticle, this can have a negative impact.

Polymers are widely used in biomedical applications. They are available in different compositions and forms which make them useful in designing specific systems [48]. Polymers of specific molecular weight can be designed and functionalized with various end groups depending on the application needed [49]. Polyethylene glycol (PEG) is a well known polymer used in biomaterials (fig. 6). PEG is soluble in aqueous solutions, non-biodegradable, and has extremely low immunogenicity, antigenicity, and toxicity [50]. For these reasons products utilizing PEG have been approved by the Food and Drug Administration [51].

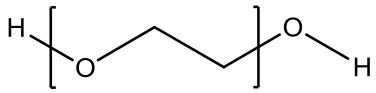

Figure 6: Chemical structure of polyethylene glycol

Of particular convenience for the stability of gold nanoparticles are alkanethiolates. The sulfur atoms in the alkanethiolates are known to have a high affinity for transition metal atoms. As such, these type of surfactants will readily adsorb to gold surfaces [52]. Using common synthetic procedures, a polymer PEG can be functionalized with a thiol end group [53]. The adsorption of such a thiolated PEG polymer to a gold surface can be completed during the synthesis of the nanoparticle itself [54, 55] or through a ligand exchange after the nanoparticle is already formed and stabilized with another ligand, such as citrate [56]. Comparison of similar alkanethiolates has shown higher physisorption enthalpies of longer chained molecules in addition to the separate chemisorption enthalpy of the sulfur-gold bond [57]. As such, DBDT, a short thiolated molecule of molecular weight 518.34 Da, can be replaced by a longer thiolated PEG with a molecular weight of 2,000 Da.

In working with thiols there is a possibility of disulfide bonds forming. In order to prevent inconsistent adsorption, disulfide bonds need to be cleaved prior to any addition to gold surfaces. Dithiothreitol (DTT) is a common reagent used to reduce disulfide bonds and maintain monothiols in the reduced state [58]. Adding DTT to solutions of alkanethiols, such as thiolated PEG, ensures that no disulfide bonds remain in the system.

Using neutral polymers such as PEG allows the nanoparticles to be sterically stable. Electrostatic stabilization is no longer a dominant factor and

therefore changes in ionic strength and pH will not cause flocculation and aggregation [59]. Additionally, nanoparticles covered with a monolayer of PEG have shown to be physiologically stable in biological systems as the PEG prevents protein adsorption which would normally occur due to electrostatic interaction [60].

Additionally, conjugating a fluorophore to a PEG polymer can be useful in later analysis through the use of fluorescent microscopy. For example, Kam, et *al.* functionalized single wall carbon nanotubes (SWNTs) with both a PEG containing a folate moiety for cellular targeting and a PEG functionalized with the covalently bound fluorophore FITC [61]. The SWNTs were internalized into the cells and consequently fluorescent microscopy showed FITC fluorescence inside the cells.

2.6. Targeting Moieties

Recent developments in cancer research have highlighted the importance of integrins. Integrins consist of a family of cell adhesion molecules that bind to the external cellular matrix and to other cell adhesion molecules. They provide signal responses both extracellularly and intracellularly. Integrins are heterodimeric glycoproteins comprised of subunits designated as alpha and beta. Multiple versions of the alpha and beta subunits have been identified and classified [62].

Research has shown an overexpression of specific integrins in cancerous cells relative to healthy cells [63]. For example, the $\alpha_v\beta_3$ integrin was found to be

overexpressed in glioblastoma multiforme [9]. Furthermore, this integrin forms cell adhesion complexes with a protein called Vitronectin. This complex can be inhibited with the addition of a peptide containing the sequence Arginine-Glycine-Aspartic Acid (RGD). The integrin forms a complex with the peptide leading to a reduction in cellular adhesion. This expression of specific integrins is not limited to glioblastoma cells, but can be found in a range of cancer cells [63].

The ability of peptides to form complexes with integrins provides a useful method for cellular targeting. A cyclic version of the peptide RGD has been applied in glioma research and has shown to be more effective than the linear counterparts. Not only do certain peptides form complexes with integrins, but they can also lead to intercellular reactions. Chatterjee, et *al*. used cyclic Arginine-Glycine-Aspartic Acid peptide functionalized with Valine, Cyclo(RGDfV), to target the $\alpha_v\beta_3$ integrin of U87 gliobastoma cells and in doing so induced apoptosis [64]. However, U-251 glioblastoma cells, which are known to not express the $\alpha_v\beta_3$ integrin, did not undergo apoptosis with the addition of the cyclo (RGDfV) peptide. Additionally, the addition of a linear RGD peptide had no comparative cytotoxicity effects relative to the cyclic peptide. The specificity of the peptide-integrin complex makes it an ideal method for selective targeting.

2.7. Cellular Uptake Moieties

In developing a nanoparticle system for biosensing, cellular targeting and adhesion complexes on the cell membrane may not be sufficient for the desired application. Incorporating a method that enables the nanoparticle to cross the

cell membrane may be needed. In this regard, several protein transduction domains (PTD) have been found that lead to the transport of molecular cargo across the cell membrane [65]. Of particular note is the PTD of the HIV gene TAT (Trans-Activator of Transcription).

A TAT peptide sequence can be synthesized for delivery to cells. Richard, et *al.* synthesized the TAT PTD sequence and added a cysteine amino acid to the N-terminus for subsequent ligation to a fluorophore, either fluorescein or Alexa Fluor 488 [66]. This peptide was added to HeLa, HepG2 and CHO cells where inhibitors were selectively added to identify the method of endocytosis. The cells were then characterized using fluorescence microscopy. Results showed that the endocytosis of the peptide relied on the clathrin pathway. Yet, there was no dependency on the caveolin pathway. This correlation changes as the peptide is conjugated to macromolecules. For example, Ferrari, et *al.* conjugated a green fluorescent protein (GFP) to a PTD of TAT [67]. This macromolecule was added to HL3T1 and CHO cells concurrently with additions of clathrin and caveolar specific labeled proteins. Fluorescence microscopy showed colocalization of the caveolar specific proteins, yet no correlation was shown with the clathrin specific proteins. This led to the conclusion that the method of endocytosis was caveolar. Drugs known to affect certain cellular structures used in the caveolar process were also added to the cells. The correlation of macromolecule uptake being affected by those cells exposed to the caveolar-specific drugs further confirmed caveolar endocytosis.

Knowing that the PTD of TAT can undergo endocytosis via either a clathrin or caveolar pathway, researchers have conjugated metallic nanoparticles to TAT peptides in order to increase cellular uptake. Berry, et *al.* conjugated TAT peptides to 5 nm tiopronin-capped gold nanoparticles and added to human fibroblast cells [68]. Samples consisting of nanoparticle conjugated with both TAT peptide and PEG, nanoparticles conjugated with PEG only, and nanoparticles conjugated with tiopronin only were also added to the cells. These nanoparticles were imaged with fluorescence microscopy, scanning electron microscopy (SEM) and transmission electron microscopy (TEM). Results showed cellular uptake of all of the different type of nanoparticles. However, those conjugated with a TAT peptide underwent a caveolar-mediated endocytosis as opposed to clathrin-mediated without the TAT peptide. Additionally, gold nanoparticles with the TAT peptide only were able to cross the nuclear membrane, whereas the gold nanoparticles with both TAT peptide and PEG were unable to cross into the nucleus due to the increased size from the PEG (5 nm to 35 nm).

This research shows that gold nanoparticles can be functionalized with a peptide containing the PTD of TAT and undergo endocytosis. While Berry, et *al.* claim this to be a caveolar process, in this instance the mechanism by which TAT undergoes endocytosis is not fully agreed upon. However, the conjugation of a PTD of TAT has proved to be an effective method of cellular uptake.

2.8. PEG-Peptide Co-functionalization

As discussed before, nanoparticles are not inherently stable in biological buffers. Adding peptides alone on the surface of gold nanoparticles can cause flocculation depending on the type of peptide and the adsorbed amount [69]. This can cause issues while attempting to functionalize nanoparticles with targeting peptides. However, combining both PEG for steric stability and peptides for specific biological functions can lead to effective nanoparticle systems. For example, Liu, et *al*., added both PEG and receptor-mediated peptides to the surface of gold nanospheres [70]. These nanoparticles were then added to increasing concentrations of salt buffer to determine their stability. Additionally, the nanoparticles were added to HeLa cancer cells to determine if the peptide receptors induced endocytosis. Results showed that a minimum amount of PEG was necessary to maintain stability with changes in ionic strength. Adding the targeting peptides alone led to flocculation of the particles. However, by using a mixed monolayer of PEG and peptides the researchers were able to maintain stability while successfully inducing cellular uptake. They were able to functionalize these particles by either adding PEG first and then adding the peptide surfactants or adding both PEG and the peptide surfactants at the same time. Of particular note was the ability of peptides to adhere to the cell membrane receptors despite being shorter in length than the coadsorbed PEG.

In characterizing nanoparticle interaction with targeted cells, one needs to determine if the nanoparticles are actually internalized or merely attached to the surface membrane. This is fairly difficult to determine using fluorescently labeled nanoparticles as fluorescence microscopy will, in both instances, show a

fluorescent overlay coincident with the cells. Fortunately, scientists have developed a method for separating the two. Trypan blue is a chemical which can quench fluorescence, but cannot cross the cell membrane of live cells or fixed cells. Therefore, researchers can add trypan blue to a system quenching any fluorescence from nanoparticles outside the cell membrane, yet not any particles inside [71]. If the same level of FITC fluorescence is observed after the addition of the trypan blue as before, then the nanoparticles are internalized.

3. AIMS

Here I present a method for *in vitro* detection of glioblastoma cells using surface enhanced Raman spectroscopy (SERS). A Raman active dithiolated linker molecule will be covalently bound to the surface of gold nanospheres to selectively create nanoparticle dimers, known to be a nanoparticle-based structure that gives rise to the highest field enhancements. The linker molecule will provide a characteristic SERS signal that can be detected using a confocal Raman microscope. The dimers will be functionalized with a mixed monolayer of polyethylene glycol (PEG) for biostability and peptides for specific cell targeting. These functionalized nanoparticle dimers will adhere to the surface of the targeted cells and cross the cell membrane. Raman spectroscopy will verify the presence of the nanoparticle dimers inside the targeted cells. The specific aims of the proposed research are broken down as follows:

Aim 1: Synthesis of gold nanoparticle dimers. Gold nanoparticles will be synthesized via addition of trisodium citrate to a heated aqueous solution of tetrachloroauric acid. DBDT, a Raman active molecule, will be added to the monomers to form dimers. The formation of Raman active gold nanoparticle dimers will be confirmed by the detection of a surface enhanced Raman scattering (SERS) signal.

Aim 2: Stabilization of gold nanoparticle dimers in physiological conditions. Thiolated PEG and cysteine-modified peptides will be bound to the surface of the dimers. The dimers will then be added to solutions of phosphate buffered saline (PBS), cell culture media, and paraformaldehyde. The stability of the gold nanoparticle dimers will be confirmed via UV-Vis spectrophotometry. Additional analytical techniques will be used to characterize the bio-functionalized nanomaterials.

Aim 3: Cellular uptake of gold nanoparticle dimers into U87 glioblastoma cells. U87 cells will be cultured and seeded on glass substrates. The cells will be incubated with fluorescently labeled gold nanoparticle dimers and subsequently be fixed and stained. Using a fluorescence quenching technique, cellular uptake of the dimers will be detected with a fluorescence microscope. The final goal will be the detection of U87 cells by Raman microscopy via identification of intracellular SERS spectra.

The development of such a nanoparticle system will provide a compelling argument for the incorporation of Raman based technology in biomedical applications. The stability and multiplexing advantages of Raman molecules make them an ideal choice for future research in the fields of bioimaging and biodetection. It is well known that absorptive capacity of the biological tissues significantly drops off approaching the near infrared (NIR). The ability to tune

the surface plasmon resonance (SPR) of Raman-based nanoparticles to frequencies within the NIR region can thus lead to significant diagnostic advantages both *in vitro* and *in vivo*. In addition, the possibility of functionalizing the nanoparticle surface with multiple moieties opens the door to customizable nanoparticles designed to specifically target a wide variety of applications. The simplicity of the synthesis and the low cost of the starting materials relatively to the amount of functionalized nanoparticles produced, points toward potential upscale manufacturing of Raman based nanoparticle systems. The introduction of such a low cost, versatile system would provide physicians a tremendous advantage in the field of therapeutics.

4. EXPERIMENTAL

4.1. Materials

DBDT, PBS, THF, 4',6-diamidino-2-phenylindole (DAPI), and paraformaldehyde were obtained from Sigma Aldrich. Tetrachloroauric acid and trisodium citrate was obtained from Fischer Scientific. FITC-PEG and CH_3O-PEG were obtained from Creative PEG works. Cyclo (RGDfC) and TAT-C peptides were obtained from Anaspec. Dulbecco's Modified Eagle Medium (MEM), Fetal Bovine Serum (FBS), MEM Non-Essential Amino Acids Solution, and MEM Sodium Pyruvate Solution were obtained from Invitrogen. U87 cells were provided by Dr. Charles Roth of the Rutgers Department of Biomedical Engineering.

4.2. Synthesis of Nanoparticles

Gold nanospheres were synthesized using a variation of the Turkevich method. 487.5 mL of 18.2 MΩ deionized water from a Millipore Milli-Q Integral 3 system was added to a 500 mL Pyrex® flat bottom flask. To this, 25 mg of tetrachloroauric acid ($HAuCl_4$) was added and stirred. The faint yellow gold solution was stirred and heated on an IKA® C-MAG HS-4 hot plate until boiling. 12.5 mL of a 1% wt (34 mM) solution of trisodium citrate ($C_6H_9O_9Na_3$) was rapidly added to the boiling solution. After a period of 15 min, the solution transitioned from light yellow to light purple as the Tetrachloroauric Acid was reduced and the gold atoms began to bond together and form spheres. After the 15 minutes, the

solution was removed from heat and allowed to cool for 2 hours. The solution was reheated to a boil for 30 seconds. The color shifted from light purple to an orange/red as the nanosphere coarsened. The solution was allowed to cool overnight. 240 mL of the solution was divided into 6 conical tubes of 40 mL each. The 6 tubes were centrifuged for 60 minutes at 6,000 g's (6,579 RPM) on a Thermo Scientific Sorvall biofuge primo centrifuge. 2 mL of precipitate from each conical tube was extracted and added to a separate conical tube.

4.3. Characterization of Nanoparticles

100 µL of 0.01M BSPP were added to a 1 mL diluted sample of the gold nanoparticles. The solution was mixed for 20 minutes to allow the BSPP to ligand-exchange with the citrate on the surface of the gold allowing the nanoparticles to be well dispersed on the grid for better characterization. 5 µL of the solution were then placed on a Formvar®/carbon reinforced copper transmission electron microscope (TEM) grid (Structure Probe, Inc) and air dried for a minimum of 30 minutes. The grid was placed in a Topcon 002B TEM to obtain particle size information. Due to the higher negative charge the gold nanoparticles did not aggregate significantly while drying on the grid surface. The size information was used in conjunction with referenced material [34] to calculate an extinction coefficient.

A 2 µL drop of sample A was placed in a Thermo Scientific Nanodrop 2000 UV-Vis spectrophotometer to obtain absorption data. These data, along

with the calculated extinction coefficient, were used to calculate the nanoparticle concentration in accordance to the Beer-Lambert Law.

4.4. Dimerization and Functionalization of Nanoparticles

The citrate-capped nanoparticles were diluted with deionized water to a concentration of 0.5 nM and designated sample A. Before dimerization of the particles, a comparative study of the effect of THF was first carried out. 10 µL of THF were added to a 1 mL sample of A. This sample, along with a separate 1 mL sample of A without THF was placed in a Fischer Scientific accuSpin 17 Micro centrifuge and centrifuged at 10,000 g's (10,200 RPM) for 5 minutes. 900 µL of clear supernatant were removed from each sample and the remaining precipitate subsequently mixed via cyclic pipetting. A 2 µL sample from each was placed in the UV-Vis spectrophotometer for characterization.

To dimerize the particles, 30 mL of sample A (0.5 nM) were placed in a Corning 50 mL conical tube. 300 µL of a 125 µM solution of DBDT in THF were added to this solution via rapid addition. Prior to the addition, the DBDT in THF solution was sonicated in a Branson 1510 sonicator for approximately 5 seconds to ensure a disperse solution. This created a 2,500:1 DBDT molecule per nanoparticle ratio. The solution was then placed on a Thermo Scientific Titer plate shaker for a time period of exactly 10 minutes. At this point, the DBDT molecules, having a higher affinity for gold then citrate, began to replace citrate via a place exchange reaction. The dithiols adsorbed to the gold surfaces and

dimers began to form. The addition of DBDT in THF increased the volume by only 1% allowing the concentration of the solution to be approximated to 0.5 nM.

Two types of PEG were added to the gold nanoparticle dimers: A thiolated methoxy PEG molecule (CH_3O-PEG-SH) (fig. 7) with a molecular weight of 2,000 Da and a thiolated PEG functionalized with the fluorophore FITC (FITC-PEG-SH) (fig. 8) with a molecular weight of 3,400 Da.

The methoxy PEG was added to provide steric stability in biological buffers while the FITC-PEG was added to enable the use of fluorescence microscopy for characterization.

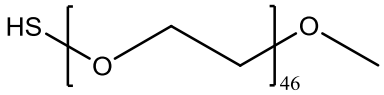

Figure 7: Chemical structure of CH_3O-PEG-SH.

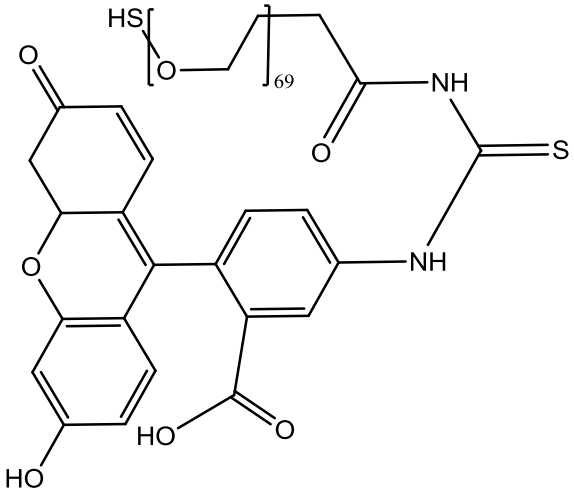

Figure 8: Chemical structure of FITC-PEG-SH.

In addition to the two PEG molecules, two peptide molecules were added: Cyclo (RGDfC) and TAT-C.

Cyclo (RGDfC) is a cysteine-modified version of the targeting peptide Cyclo (RGD) that forms a complex with the $\alpha_v\beta_3$ integrins expressed on U87 glioblastoma cells.

Cyclo (-Arg-Gly-Asp-D-Phe-Cys) MW = 599.9 Da

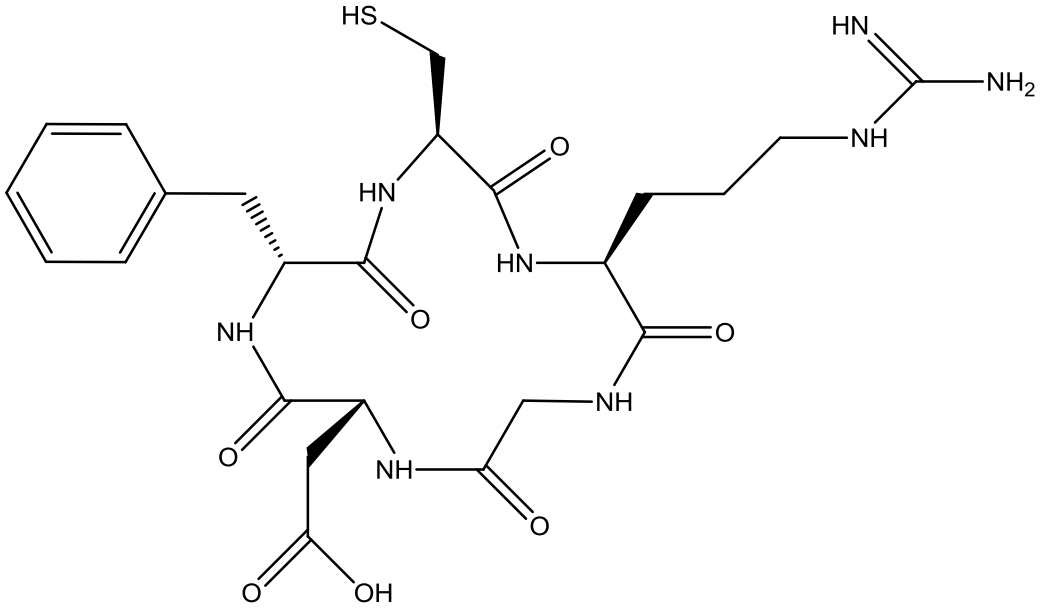

Figure 9: Chemical structure of cyclo (RGDfC).

TAT-C is a cysteine-modified version of the TAT peptide that promotes cell membrane transference.

H-Cys-Gly-Arg-Lys-Lys-Arg-Arg-Gln-Arg-Arg-Arg-OH MW = 1498.7 Da

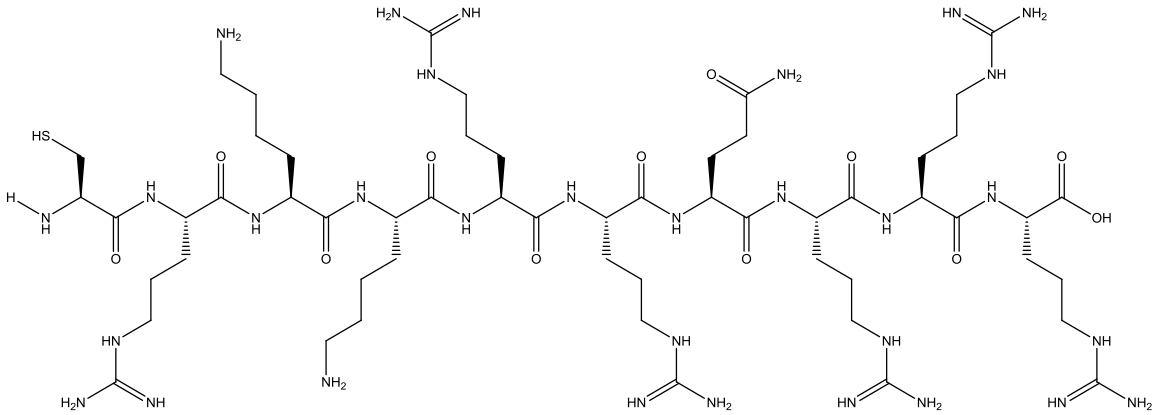

Figure 10: Chemical structure of TAT-C.

Cleland's reagent was added to the PEG and peptide solutions prior to any additions to the nanoparticles. This reagent consists of micro sized beads containing DTT, a chemical whose function in cleaving disulfide bonds has been described in Chapter 2, immobilized on the surface. 0.1 mg/mL DTT was added to 1 mg/mL CH3O-PEG and 1 mg/mL FITC-PEG solutions. 0.01 mg/mL DTT was added to 100 μM Cyclo (RGDfC) and 50 μM TAT-C solutions. All solutions were mixed for 15 minutes to allow the DTT to remove any of the disulfide bonds that may have formed from the thiol end groups.

These solutions were centrifuged at 5,000 g's (7,200 RPM) for 5 minutes. 90% volume of supernatant was separated from the 10% precipitate containing the beads. The supernatant was subsequently centrifuged again to remove any remaining beads not removed in the first centrifugation. In total, the solutions were centrifuged three times to ensure that none of the Cleland's reagent remained in the PEG and peptide solutions.

After the gold nanoparticle dimer solution was mixed for 10 minutes, it was separated into six samples. The PEG and peptide surfactants were added in accordance to the table below.

Sample	Gold Nanoparticles (0.5 nM)	DBDT in Sample (Molar Ratio)	Addition of CH_3O-PEG (Molar Ratio)	Addition of FITC-PEG (Molar Ratio)	Addition of Cylco (RGDfC) (Molar Ratio)	Addition of TAT-C (Molar Ratio)
B	2 x 1 mL	2,500x	None	None	None	None
C	8 mL	2,500x	7,500x	2,500x	None	None
D	8 mL	2,500x	7,500x	2,500x	2,500x	None
E	8 mL	2,500x	7,500x	2,500x	2,500x	100x
F	2 x 1 mL	2,500x	None	None	2,500x	None
G	2 x 1 mL	2,500x	None	None	2,500x	100x

Table 1: PEG and peptide additions to gold nanoparticle dimers.

The reactions of C, D, and E were carried out in 16 mL glass vials. The reactions of B, F, and G were carried out in 1.5 mL Eppendorf tubes. In all cases the reactants were added to the dimer solution rapidly with a sequence priority of CH_3O-PEG-SH, FITC-PEG-SH, Cyclo (RGDfC) and TAT-C. Once added, the sulfur atoms in the thiol and cysteine groups began to adsorb to the gold. Due to a higher binding affinity, the PEG/peptide surfactants began to replace the DBDT molecules on the surface of the particles. However, because of the relatively larger sizes of the PEG and peptides, the new surfactants were unable to reach the small gap between the dimerized nanoparticles allowing the DBDT molecules at those junction points to remain bound.

The 1 mL samples were shaken in a Fischer Scientific microtube thermal mixer at 1,400 RPM for a period of 2 hours. The 8 mL samples were placed on

the Titer shaker and mixed at setting of 2 for 2 hours. After that time, 7 x 1 mL samples of C, D and E were transferred to 1.5 mL Eppendorf tubes along with a 1 mL samples of B, F, and G centrifuged at 1,500 g's (4,000 RPM) for 1 hour in the microcentrifuge. 900 µL of the supernatant were removed and the remaining 100 µL precipitates from each sample was consolidated.

Separately, 20 µL of a 125 µM solution of DBDT in THF was rapidly added to 200 µL (0.5 nM) of sample A creating a molar ratio of 25,000:1. This sample was designated H and mixed in the thermal mixer for 2 hours. The sample was then centrifuged at 5,000 g's (7,200 RPM) for 5 minutes. 90% of the supernatant was removed and 2 µL of the remaining precipitate were observed in the UV-Vis spectrophotometer.

Additionally, 100 µL of a 100 µM solution of DBDT in THF was rapidly added to 1 mL (0.5 nM) of sample A creating a molar ratio of 20,000:1. This sample was designated I and mixed in the thermal mixer for 2 hours. The solution was then set aside for 2 weeks. The sample was then centrifuged at 5,000 g's (7,200 RPM) for 5 minutes. 90% of the supernatant was removed and 2 µL of the remaining precipitate were observed in the UV-Vis spectrophotometer.

Sample	Gold Nanoparticles	DBDT in Sample (Molar Ratio)	Time between synthesis and UV-Vis spectroscopy
B	0.5 nM	2,500x	< 1 Day
H	0.5 nM	25,000x	< 1 Day
I	0.5 nM	20,000x	> 2 Weeks

Table 2: DBDT additions to gold nanoparticles.

Three days after the synthesis of the nanoparticles, 10 µL of a 50 µM solution of TAT-C were added to a 50 µL (0.5 nM) diluted sample of C creating a TAT-C to gold nanoparticle ratio of 20,000x. This sample was designated J and mixed for 2 hours on the thermal mixer. This sample was then centrifuged at 5,000 g's (7,200 RPM) for 5 minutes. 90% of the supernatant was removed and a 2 µL aliquot from the remaining precipitate was observed in the UV-Vis Nanodrop spectrophotometer.

4.5. Characterization of Functionalized Nanoparticles

2 µL aliquots of samples A through G were placed in the UV-Vis Nanodrop spectrophotometer for characterization. The UV-Vis data along with the aforementioned extinction coefficient was used to calculate the concentration of the samples. 400 µL aliquots of samples A through G at 0.5 nM concentration were characterized in a Malvern DTS Nano zetasizer (633 nm wavelength) to determine effective hydrated particle diameter. A 5 µL aliquot of sample E at 0.025 nM concentration was placed on a TEM grid and dried for a minimum of 30 minutes. The grid was subsequently observed in the Topcon 002B TEM to determine the presence of nanoparticle dimers and trimers.

50 µL of approximately 5 nM concentration of sample E were added to 450 µL of 4% wt. paraformaldehyde. This sample was designated K and mixed for 3 hours on the thermal mixer. The sample was then set aside for 15 hours. This sample was then centrifuged at 10,000 g's (10,200 RPM) for 10 minutes. 450 µL of the supernatant was removed and 450 µL of deionized water was

added. The sample was then centrifuged again at 10,000 g's (10,200 RPM) for 10 minutes. 450 µL of the supernatant was removed and a 2 µL aliquot of the remaining precipitate was observed in the UV-Vis Nanodrop spectrophotometer.

5 µL aliquots of samples A, C, D, E and K at 0.5 nM concentration were dried on a glass slide and observed with a Reinshaw inVia Raman microscope using a 50 mW 633 nm HeNe laser. As controls, a small amount of DBDT powder and a 5 µL aliquot of DBDT in THF at 11.5 µM concentration was placed on a glass slide and also observed in the Raman microscope.

4.6. Stability of Functionalized Nanoparticles

9 µL of approximately 5 nM from each sample were added to 1 µL of 10x Phosphate buffered saline (PBS). 2 µL aliquots from each sample were characterized with the UV-Vis Nanodrop spectrophotometer.

20 µL aliquots of approximately 5 nM concentration of samples C, D, and E were added to 80 µL of a cell culture media. This media consisted of Dulbecco's Modified Eagle Medium (D-MEM) (high glucose) with 10% Fetal Bovine serum (FBS), 1% penicillin/streptomycin, 1% Non-Essentially Amino Acid Solution and 1% Sodium Pyruvate. These samples were mixed at 1,400 RPM for 15 minutes on the thermal shaker. The samples were then centrifuged at 4,000 g's (6,500 RPM) for 15 minutes in the microcentrifuge. 80% of the supernatant was removed and replaced with deionized water. The samples were again centrifuged at 4,000 g's (6,500 RPM) for 15 minutes. Again, 80% of the

supernatant was removed. The samples were centrifuged a third time at 4,000 g's (6,500 RPM) for 15 minutes. 80 % of the supernatant was removed and 2 µL of the remaining precipitate was characterized via UV-Vis spectroscopy.

4.7. Cell Culture

U87 cells were obtained from Rutgers department of Biomedical Engineering. The cells were grown in a DB Falcon 25 cm^2 treated tissue culture flask with the aforementioned cell culture media and incubated in a Thermo Electron Corporation Forma Series II water jacketed incubator at 37^oC and 5% CO_2. Every two to three days, the media was removed from the flask with an aspirator and replaced with 5 mL of fresh media with a pipette. Cells were observed using an Olympus CKX31 optical microscope. After the cells reached 70% confluence, they were split. For the splitting procedure, the media was first removed from the flask with an aspirator. 1 mL of 1x PBS was then added and subsequently removed to wash the cells. Next, a 1 mL solution to Trypsin-EDTA was added and subsequently removed coating the cells. The cells were placed in the incubator for 1 minute and 30 seconds to allow the remaining Trypsin-EDTA to strip the cells from the surface of the flask. 5 mL of cell culture media was then added to the flask to create a colloidal solution of cells. A 100 µL sample was removed and added to a 100 µL sample of 0.4% volume Trypan Blue and mixed to stain any dead cells. A 10 µL drop of this solution was added to a Hemocytometer to determine a cell count. This cell count was used to determine the concentration of cells in the flask.

To maintain the cell line, 300 µL to 500 µL aliquots were added to 4.5 mL of cell culture media in a new 25 cm^2 treated tissue culture flask. Once this flask reached 70% confluence, the cells were split again.

In establishing cell samples for experiments, MatTek ploy-d-lysine treated 14mm glass bottom - 35mm Petri dishes and BD Falcon™ 12-well treated polystyrene cell culture plates were used. Using the concentration of cells determined from the Hemocytometer, the Petri dishes and culture plates were seeded with a surface concentration of 40,000 cells per cm^2. The cells suspended in the cell culture medium were allowed to adhere to the poly-d-lysine surfaces for 18 hours before any addition of nanoparticles.

4.8. Addition of Functionalized Nanoparticles to U87 Cells

A 12-well cell culture plate was seeded at 40,000 cells/cm^2 during passage 10. Three glass bottom Petri dishes were seeded at 40,000 cells/cm^2 during passage 17 and designated C_1, D_1, and E_1. Three additional Petri dishes were seeded at 40,000 cells/cm^2 during passage 18 and designated C_2, D_2, and E_2.

150 µL of an 8 µM solution of FITC-PEG were added to 450 µL of media. This FITC control solution was added to a well in the 12-well cell culture plate to determine if the cells will uptake unbound FITC-PEG molecules. This created a FITC-PEG molecule to cell ratio of approximately 1.6×10^{10}:1.

100 µL of the 5 nM solutions of C, D, and E were added to 900 µL of media and mixed. These solutions were added to the Petri dishes C_1, D_1, and

E_1. This was repeated for Petri dishes C_2, D_2, and E_2. This 0.5 nM nanoparticle solution created a gold nanoparticle to cell ratio of approximately 2 x 10^6.

Sample	Gold Nanospheres (5 nM)	Media	Nanoparticle to Cell Ratio
C_1	100 µL	900 µL	2,000,000x
D_1	100 µL	900 µL	2,000,000x
E_1	100 µL	900 µL	2,000,000x
C_2	100 µL	900 µL	2,000,000x
D_2	100 µL	900 µL	2,000,000x
E_2	100 µL	900 µL	2,000,000x
FITC-PEG Control (8 µM) (150 µL)	0 µL	450 µL	Equivalent to 6,400,000x of nanoparticles with 2,5000x FITC-PEG

Table 3: Nanoparticle additions to U87 cells.

After the addition of the FITC-PEG, the 12-well cell culture plate was incubated for 24 hours. After the addition of the nanoparticles, the Petri dishes were incubated for 3 hours. After incubation, both the well plate and Petri dishes were fixed.

To fix the cells, the media/nanoparticle solutions were gently removed using a pipette. Then, 1 mL of 1x PBS was added and removed three times to wash out any remaining media/nanoparticles. 800 µL of cold 4% wt paraformaldehyde were then added to the cells. After allowing 20 minutes for the cells to be fixed, the paraformaldehyde was removed. 1 mL of deionized water was added and removed three times to wash out any remaining paraformaldehyde. Then, a solution of DAPI just sufficient to cover the cells was added to stain the nucleus. After 5 minutes, the DAPI solution was removed and

1 mL of deionized water was added and removed three times to wash out any remaining DAPI. 1 mL of water was added and left in the well plate and 2 mL of water was left in the Petri dishes.

4.9. Characterization of U87 Cells

Within 3 hours of fixing, the cells in the 12-well cell culture plate were observed in a Nikon Eclipse TE2000-S fluorescence microscope to determine if the FITC-PEG molecules underwent endocytosis.

Within 3 hours of fixing, the cells in C_1, D_1, and E_1 were observed in a Leica DMIRE2 fluorescent microscope using Leica Confocal software. Any concurrence of the FITC labeled nanoparticles and the DAPI labeled cells was observed. Then, the deionized water from C_1, D_1, and E_1 was removed with a pipette and replaced with 1 mL of 0.05% trypan blue. The cells were again observed in the fluorescent microscope.

Within 3 hours of fixing, the cells in C_2, D_2, and E_3 were observed in the Reinshaw inVia Raman microscope at 50x magnification with a 50 mW 633 nm HeNe laser to determine the presence of any SERS signal. The energy of the laser beam increased the rate of evaporation and the cell slowly began to dry out as they were observed. One week after the fixing the cells, sample E_2 was again observed in the Raman microscope to determine the presence of any SERS signal.

5. RESULTS

5.1. Synthesis and Characterization of Nanoparticles

The initial reaction of the gold particles yielded a light purple color indicative of smaller (<20nm) particles. To obtain nanoparticles in the desired 20 nm to 30 nm range, the solution was reheated to a boil and the color shifted to an orange/red as the particles coarsened to a larger size. The nanoparticles were then purified via centrifugation. Previous experiments had indicated a tendency for the nanoparticles to irreversibly aggregate on the bottom of conical tubes at high centrifugation force. 6,000 g's for 60 minutes was found to be a sufficient amount of force and time to create a fairly clear supernatant without excessive aggregation and loss of samples.

Replacing the citrate with a monolayer of BSPP increased the negative surface charge and prevented the usual excessive aggregation that occurs with the drying of citrate gold nanoparticles on TEM grids. Micrographs obtained using Digital Micrograph software shows a prevalence of gold nanospheres (figs. 11 and 12).

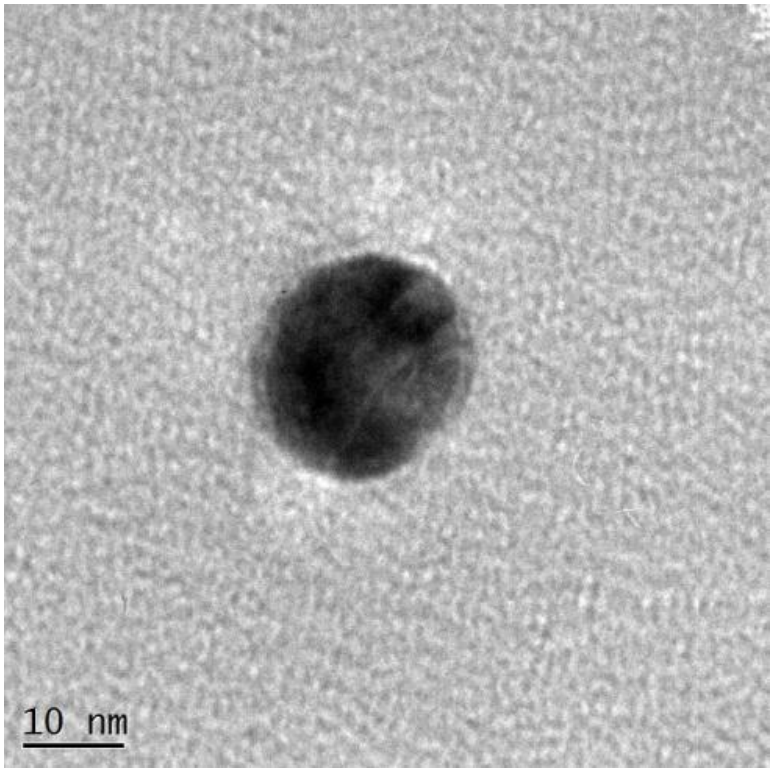

Figure 11: TEM micrograph of a gold nanosphere.

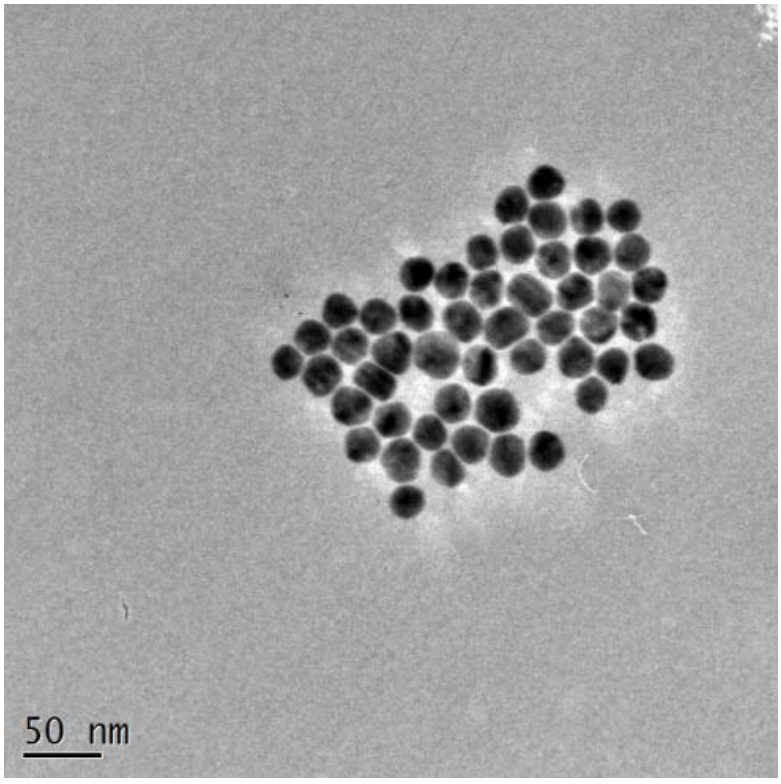

Figure 12: TEM micrograph of gold nanospheres.

The average diameter of the nanoparticles was estimated to be 24.2 ± 2.2 nm over a sample of more than 200 particles (fig. 13).

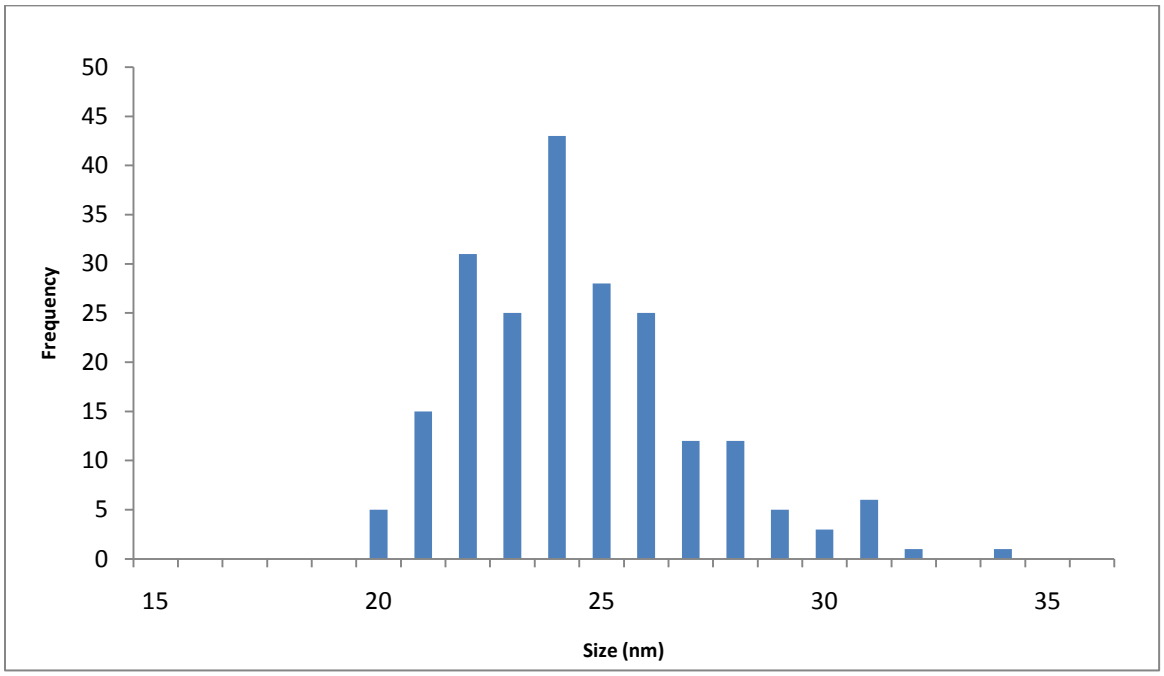

Figure 13: Size distribution histogram of gold nanospheres.

Using the previously discussed equation developed by Xiong Liu, et *al*. [34] for citrate capped gold nanoparticles in water; an extinction coefficient of 1.95 x 10^8 mm^{-1} M^{-1} was estimated.

$$\ln \varepsilon = 3.32111 \cdot \ln(24.2) + 10.80505 \qquad \varepsilon = 1.95 \text{ x } 10^8 \text{ mm}^{-1} \text{ M}^{-1}$$

UV-Vis spectrophotometry showed an absorption peak at 523 nm attributed to a surface plasmon resonance band (fig. 14).

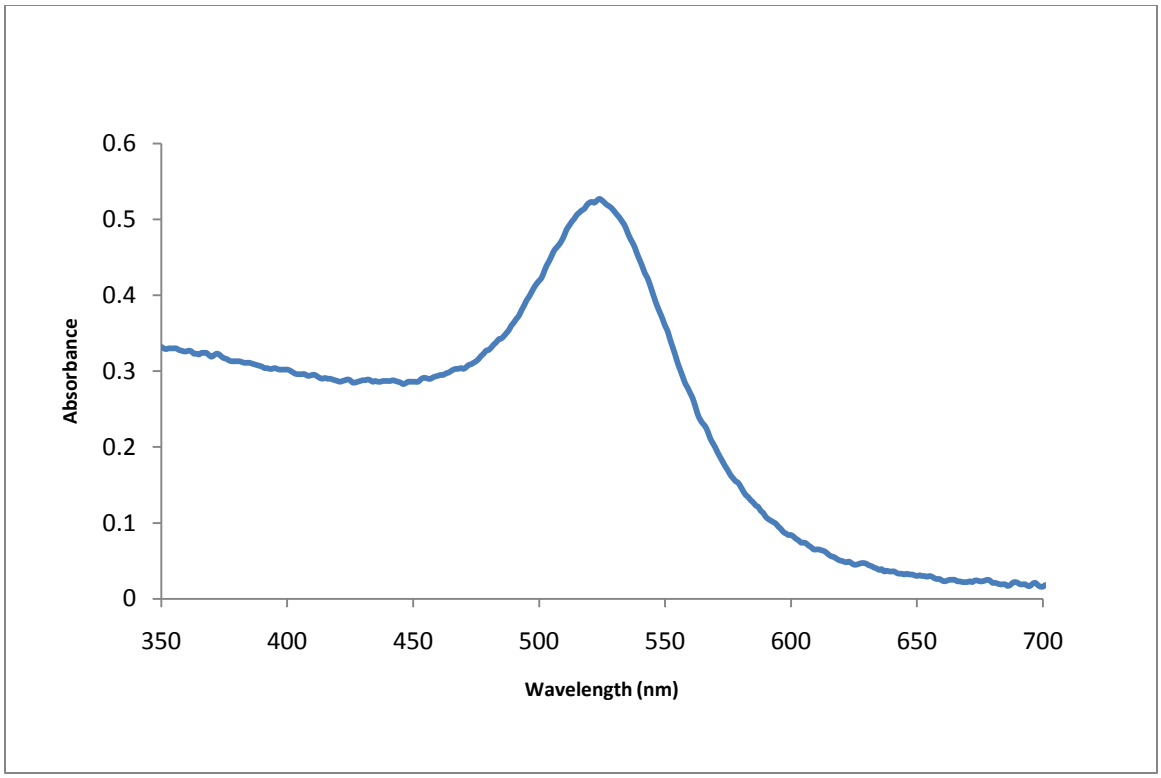

Figure 14: Absorption spectra of gold nanospheres.

5.2. Dimerization and Functionalization of Nanoparticles

A UV-Vis spectra comparison of gold nanoparticles with and without 1% volume THF showed a slight shift of 1-2 nm after the THF was added (fig. 15). This shift was expected as theoretically predicted and attributed to the effect of the dielectric constant.

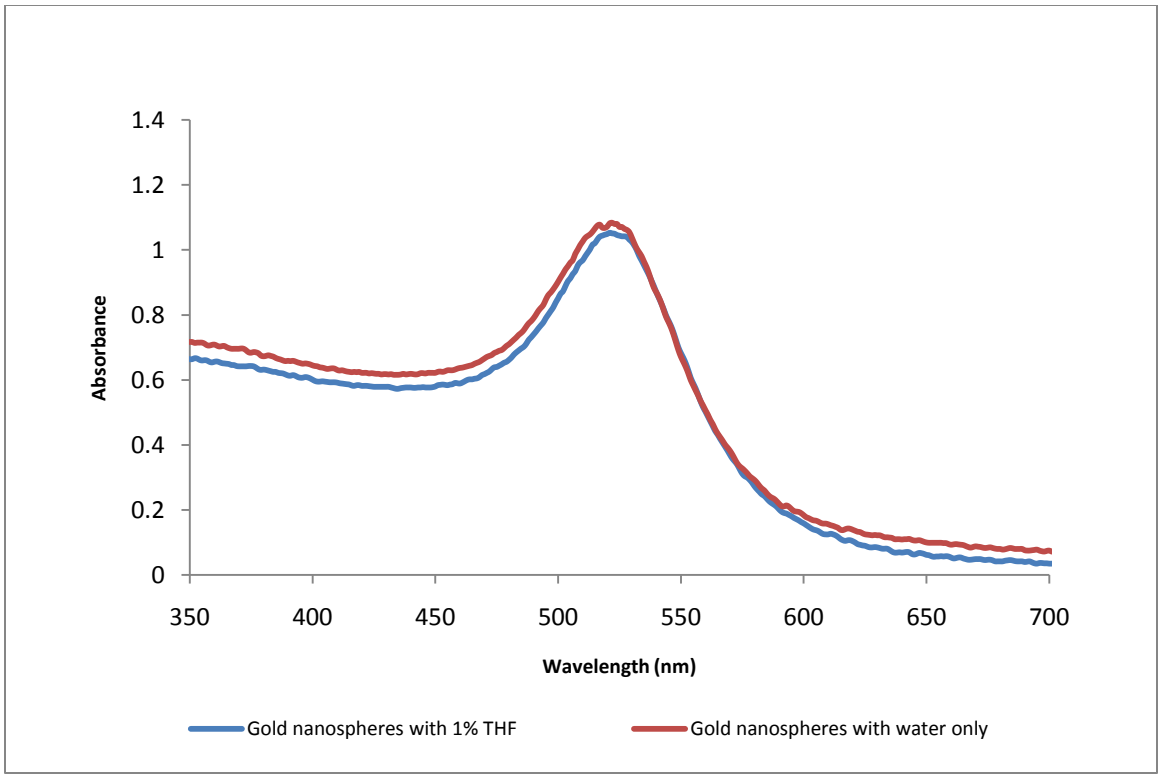

Figure 15: Absorption spectra of gold nanoparticles with and without 1% volume THF.

After the addition of DBDT there is an approximately 6 nm shift of the SPR caused by the change in the dielectric constant of surrounding medium and the additional plasmon coupling created as the monomers formed into dimers and trimers (fig. 16). The orange/red color of the monomer solution shifted to a slightly darker orange/red color. Due to differences in concentration, the peak absorbance values of the samples are not coincident in the UV-Vis spectra. The plasmon shift induced by the addition of DBDT in THF, 6 nm, compared to THF only, 2 nm, indicates the formation of dimers and the generation of plasmon coupling. It is of note that B was observed on the same day as the synthesis.

If a higher molar concentration of DBDT is added, such as 25,000x for sample H, the plasmon shift will increase to 11 nm (fig. 16). If these particles are

not capped with other surfactants, over time the dithiolated nature of the DBDT will cause the continuous growth of larger multi-*mer* particle aggregates in the solution. This occurred in sample B as it slowly shifted from orange/red color on the day of synthesis to a blue color 5 days later as agglomerates began to form. The degree of aggregation is dependent on the amount of DBDT added and the elapsed time. This can be seen by an even larger 20 nm plasmon shift of a 20,000x molar concentration, sample I, after two weeks (fig. 16). The formation of multi-*mer* complexes in H can be deduced by the inconsistent absorption spectra rising from changes in the plasmonics properties in the 600 nm to 700 nm range as observed over multiple samplings (fig. 17).

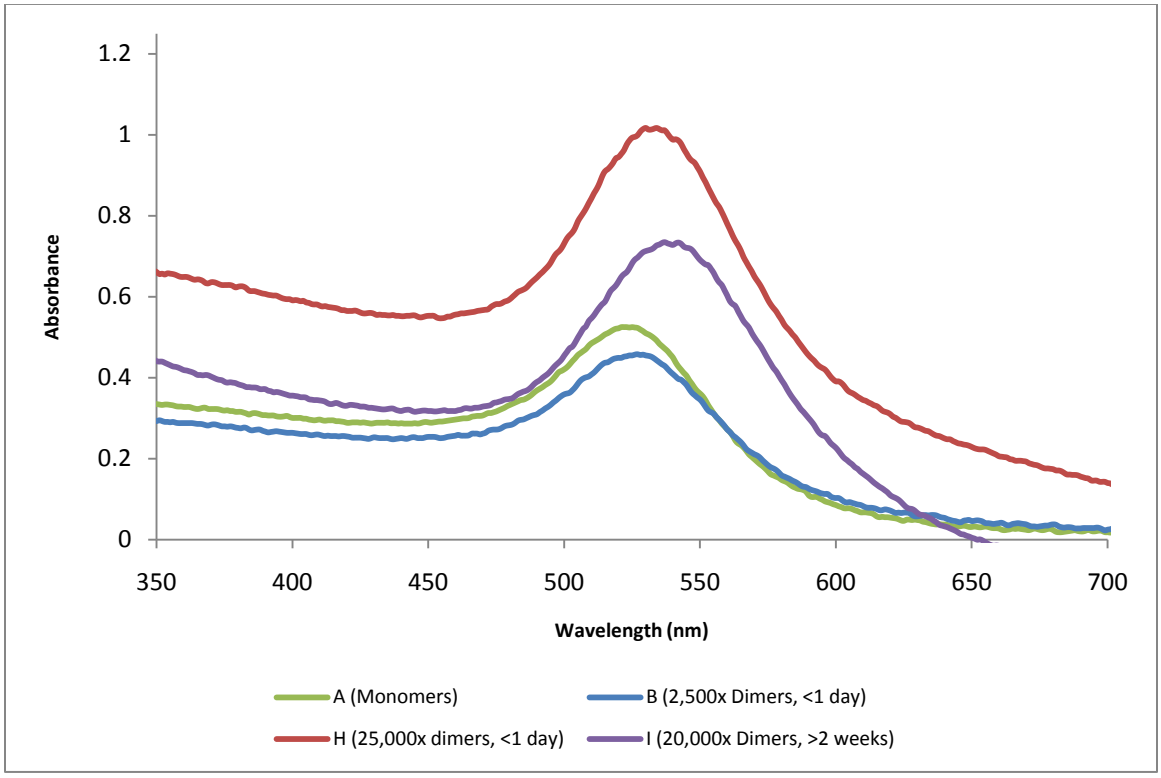

Figure 16: Plasmon shifts induced by addition of DBDT and subsequent nanoparticle assembly.

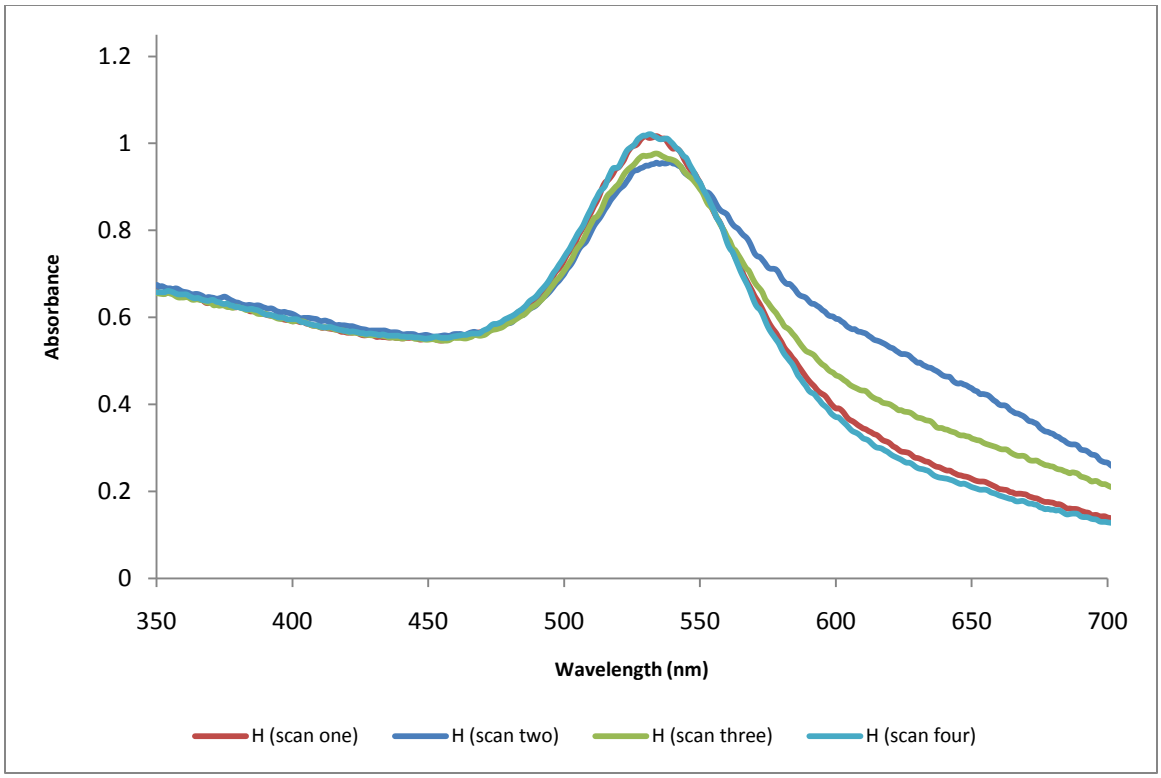

Figure 17: Inconsistent absorption spectra of multi-*mer* gold nanoparticles.

Adding PEG and peptides after 10 minutes caused a ligand exchange with the DBDT which lead to the removal of the dithiolated molecules from the surface of the nanoparticles with the exception of those at the junctions. This limited the particle aggregation to mainly dimers and trimers. A consistent 6 nm plasmon shift is observed when comparing the nanosphere monomers of A and the PEG/peptide stabilized nanospheres of C, D, and E (fig. 18).

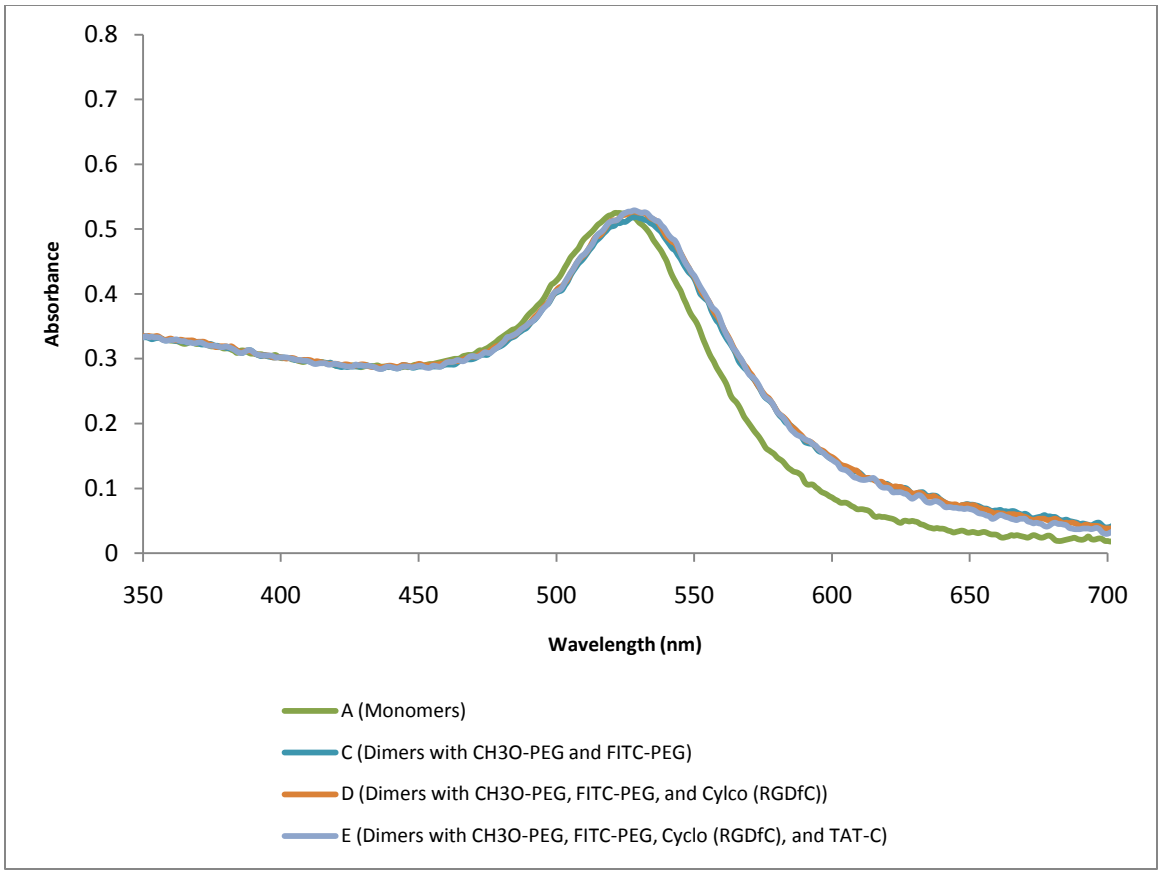

Figure 18: Absorption spectra of gold nanoparticles monomers and dimers stabilized with PEG and peptides.

The amount of TAT-C peptide added to sample E was limited to 100x due to the tendency of the nanoparticles to flocculate and fall out of solution at higher TAT-C concentrations. TAT-C was found to have a strong binding affinity to the gold surface even at low ratios relative to CH_3O-PEG and FITC-PEG.

Adding cyclo (RGDfC) without PEG, sample F, also led to an approximately 6 nm shift. However, when incorporating 100x TAT-C into the solution, sample G turned from an orange/red to a blue color. This color shift indicated the formation of aggregates in the solution. Some small black aggregates were observed in the Eppendorf tube after the sample was

centrifuged after the reaction. This aggregation was confirmed by UV-Vis spectroscopy as sample G showed the rise of a second plasmon in the 600 nm to 700 nm range (fig. 19). Therefore, while adding 100x TAT-C to gold nanoparticles concurrently with PEG does not lead to flocculation, adding 100x TAT-C to gold nanoparticles without PEG will.

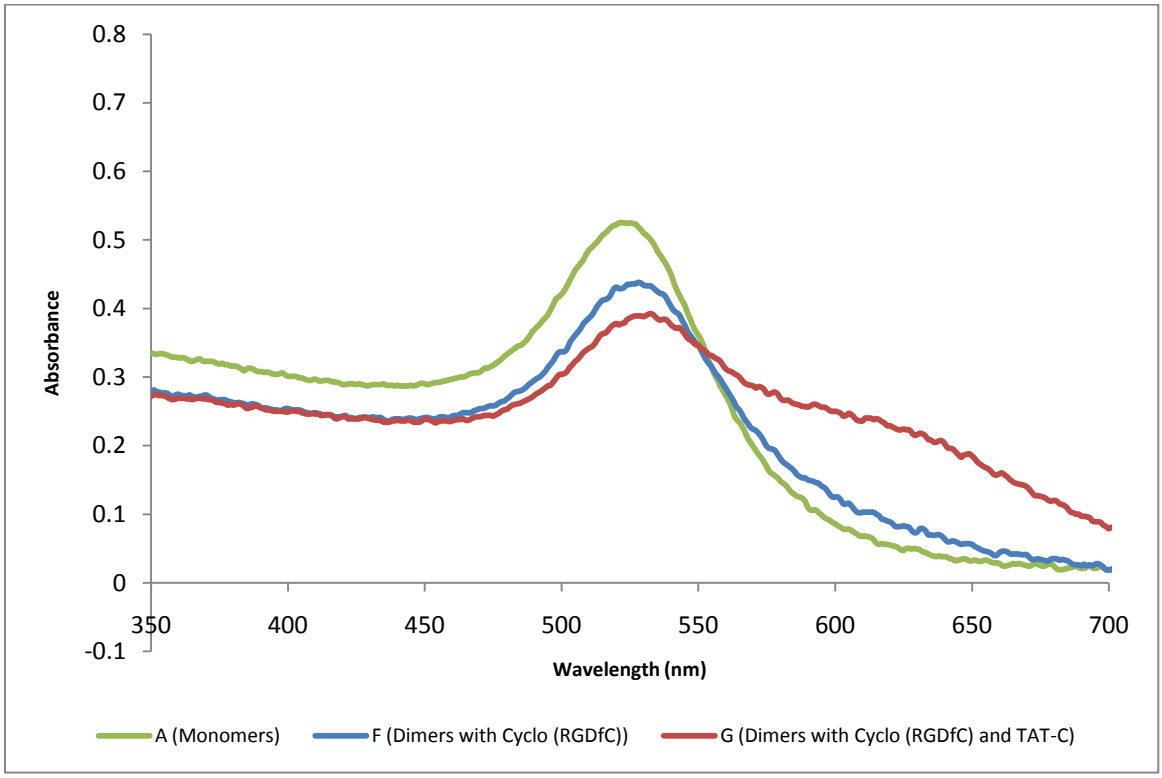

Figure 19: Absorption spectra of gold nanoparticle monomers stabilized with peptides only.

Adding both the PEG and peptides at the same time allowed the formation of a mixed monolayer. However, if PEG is added to the solution first, and forms a PEG only monolayer, TAT-C will not be able to adsorb to the gold surface. Adding 20,000x TAT-C to a gold nanoparticle solution with a PEG monolayer, sample J, did not lead to aggregation or any change in the SPR (fig. 20). This

happened despite the aggregation that began to occur at molar ratios greater than 100x when the TAT-C was added simultaneously with PEG.

Adding paraformaldehyde to sample E did not cause flocculation of the solution. Instead, the absorption spectra of sample K showed a 2 nm blue shift in the SPR (fig. 21). This was due to a change in the dielectric constant of the medium.

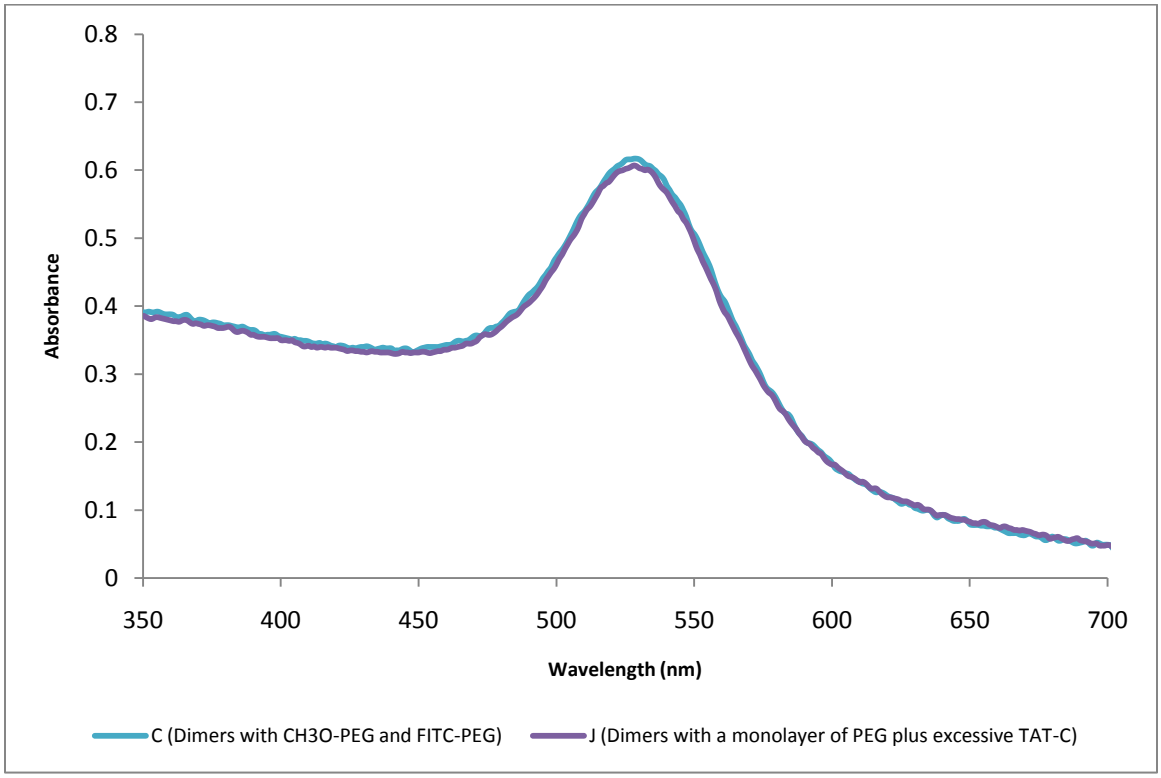

Figure 20: Absorption spectra of gold nanoparticle dimers with PEG before and after excessive TAT-C.

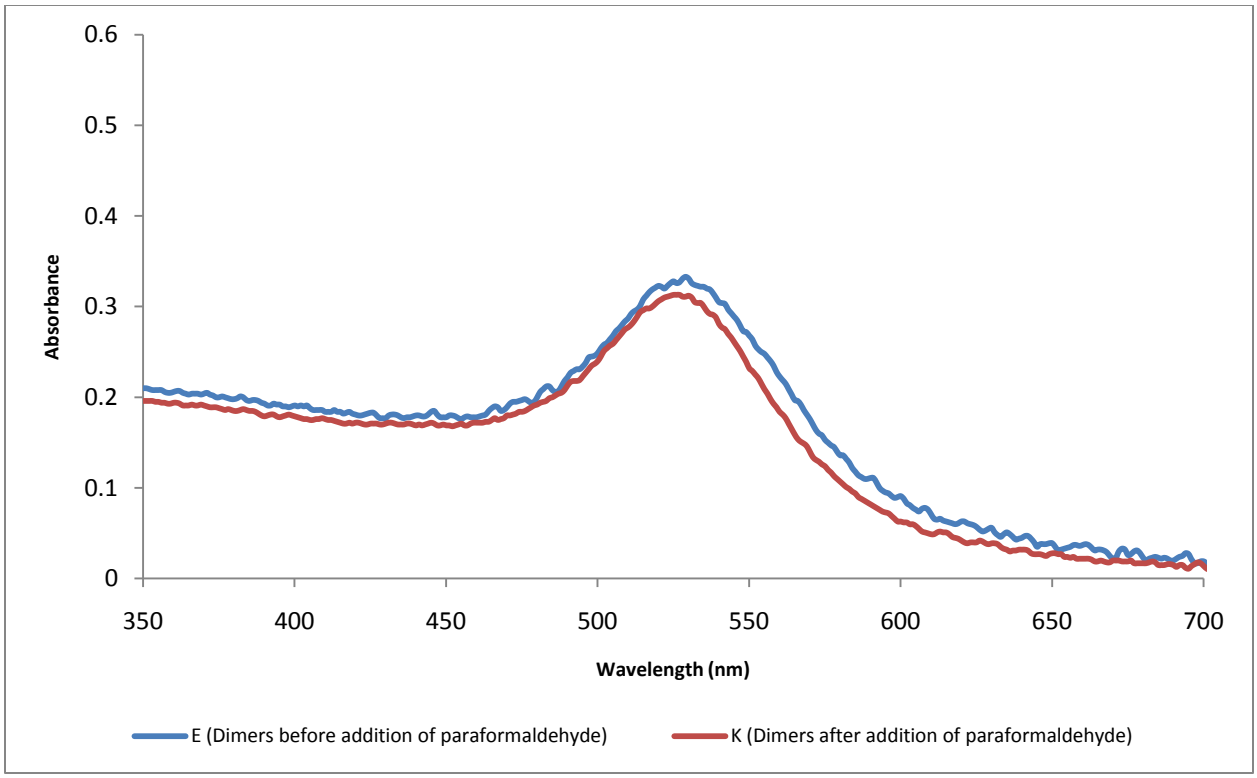

Figure 21: Absorption spectra of gold nanoparticle dimers before and after paraformaldehyde.

Sample	A	B	C	D	E	F	G	H	I	J	K
SPR Peak λ (nm)	523 ± 1	528 ± 1	528 ± 1	528 ± 1	528 ± 1	528 ± 1	528 ± 1	534 ± 1	542 ± 1	526 ± 1	528 ± 1

Table 4: SPR peaks of nanoparticle samples

5.3. Characterization of the Functionalized Nanoparticles

5.3.1. Zetasizer:

A zetasizer uses light scattering techniques to measure the effective hydrodynamic diameter of nanoparticles. Data from a zetasizer confirmed the adsorption of the surfactants on the gold nanoparticles as indicated by the changes in the effective diameter, Z_{AVG}:

Sample	**A:** Monomers	**B:** Dimers	**C:** PEG	**D:** PEG Cylco (RGDfC)	**E**: PEG Cylco (RGDfC) TAT-C	**F:** Cyclo (RGDfC)	**G:** Cylco (RGDfC) TAT-C
Z_{AVG} (nm)	29.6 ± 0.2	30.2 ± 0.2	54.8 ± 0.3	51.1 ± 0.3	47.4 ± 0.1	30.8 ± 0.2	56.6 ± 0.3

Table 5: Effective hydrodynamic diameters.

Due to the formation of dimers there is a slight increase in the average diameter from A to B. This size is drastically increased as PEG adsorbs onto the dimers, C. Because of the shorter length of Cyclo (RGDfC) and TAT-C relative to PEG, the average diameters of nanoparticle with mixed monolayers, D and E, are both shorter than C. The adsorption of Cyclo (RGDfC) is observed by a slight increase from B to F. As discussed before, adding TAT-C without PEG can cause the formation of aggregates, as observed by the large average diameter of G relative to F.

5.3.2. Raman Spectroscopy:

The presence of SERS signals from DBDT was investigated with a Reinshaw InVia confocal Raman microscope. The samples were scanned at 10% power using a 633 nm laser. There are Raman peaks specific to DBDT as observed by the spectra obtained from the dry powder (fig. 22). However, when diluted in THF to a concentration of 11.2 μM, these peaks are no longer observable (fig. 23). Gold nanoparticle monomers without DBDT, sample A, will have broad, noisy peaks (fig 24) whereas, the adsorption of DBDT to gold will result in distinct SERS spectra as indicated by the dried samples of C, D, and E

(figs. 25 through 27). Adding paraformaldehyde to the nanoparticle dimers will not degrade the SERS spectra as indicated by the dried sample of K (fig. 28).

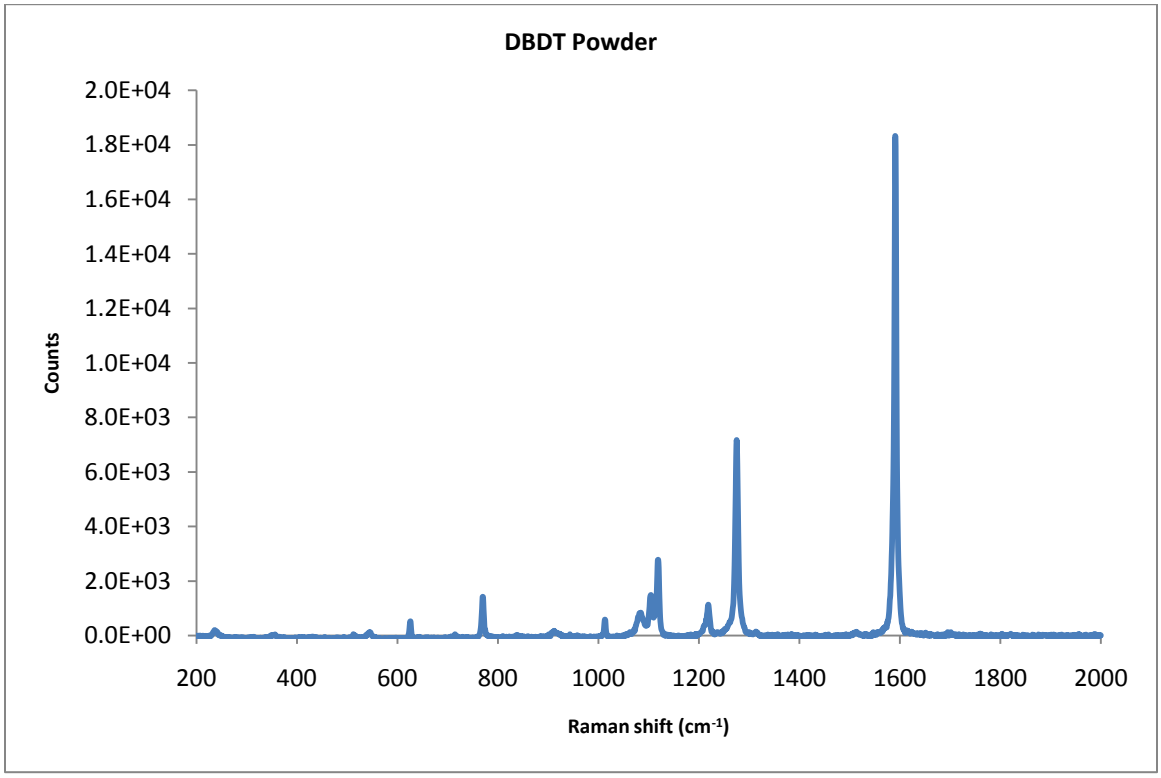

Figure 22: Raman spectrum of DBDT powder.

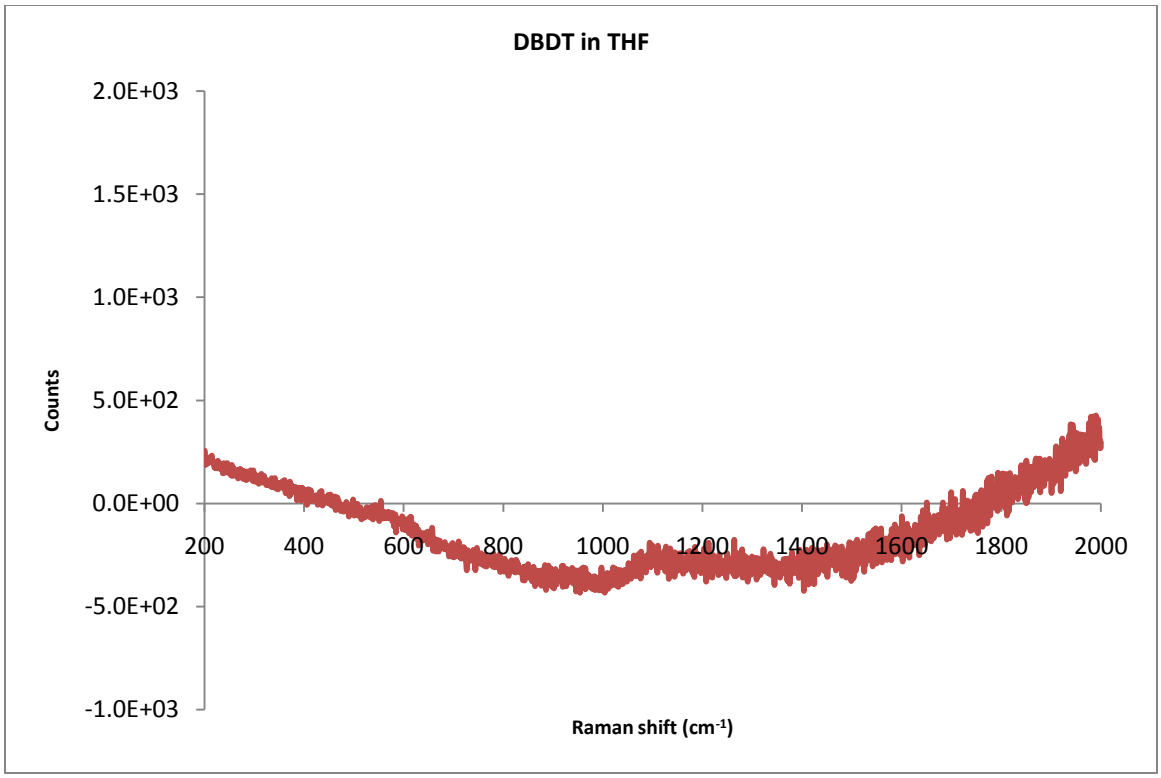

Figure 23: Raman spectrum of DBDT in THF.

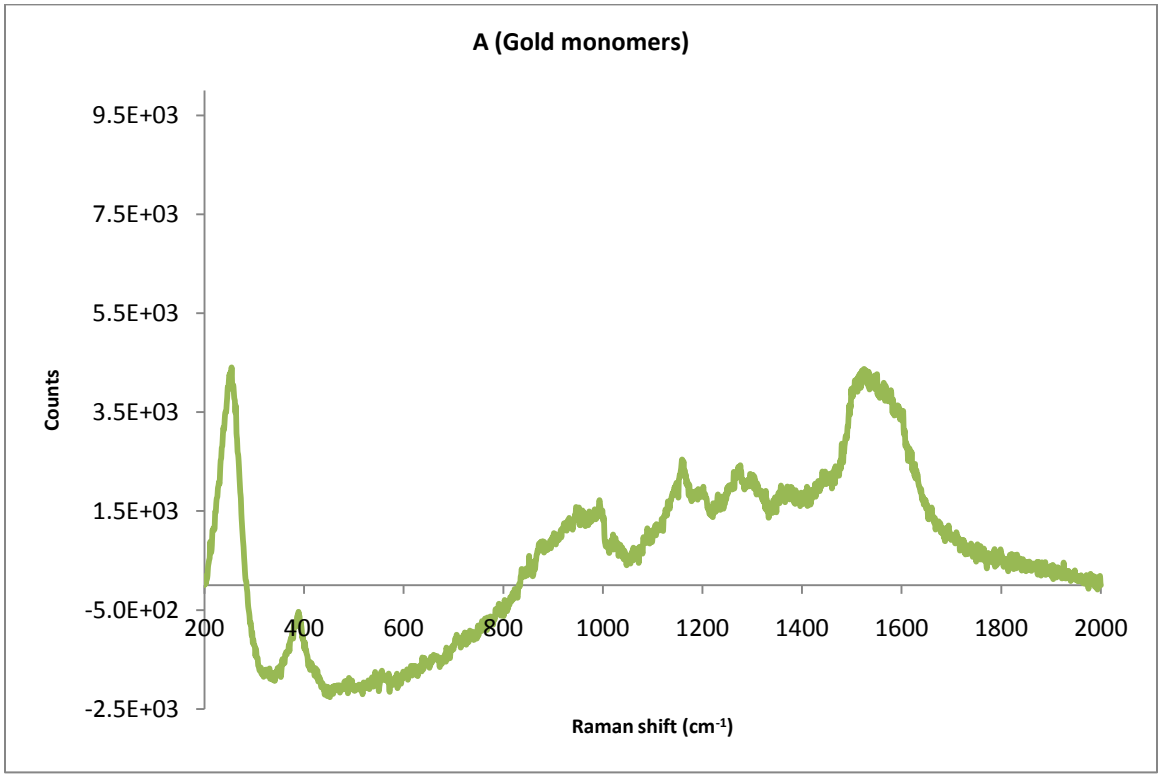

Figure 24: Raman spectrum of sample A.

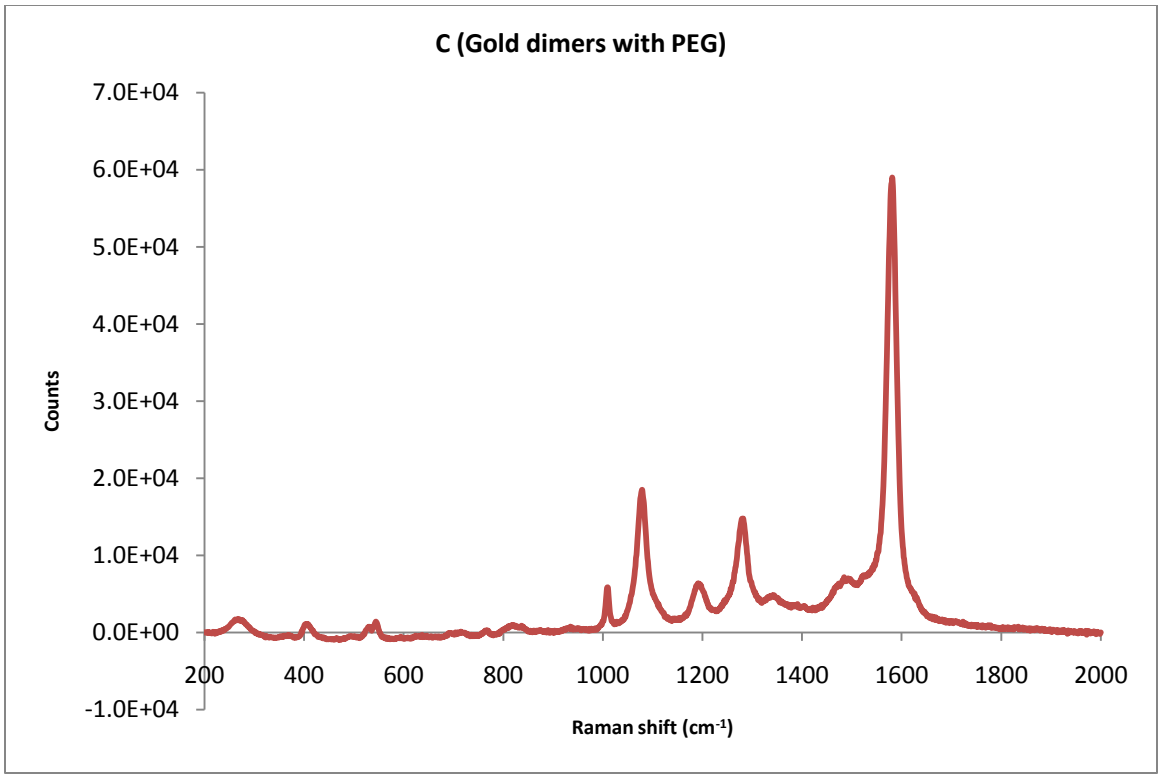

Figure 25: Raman spectrum of sample C.

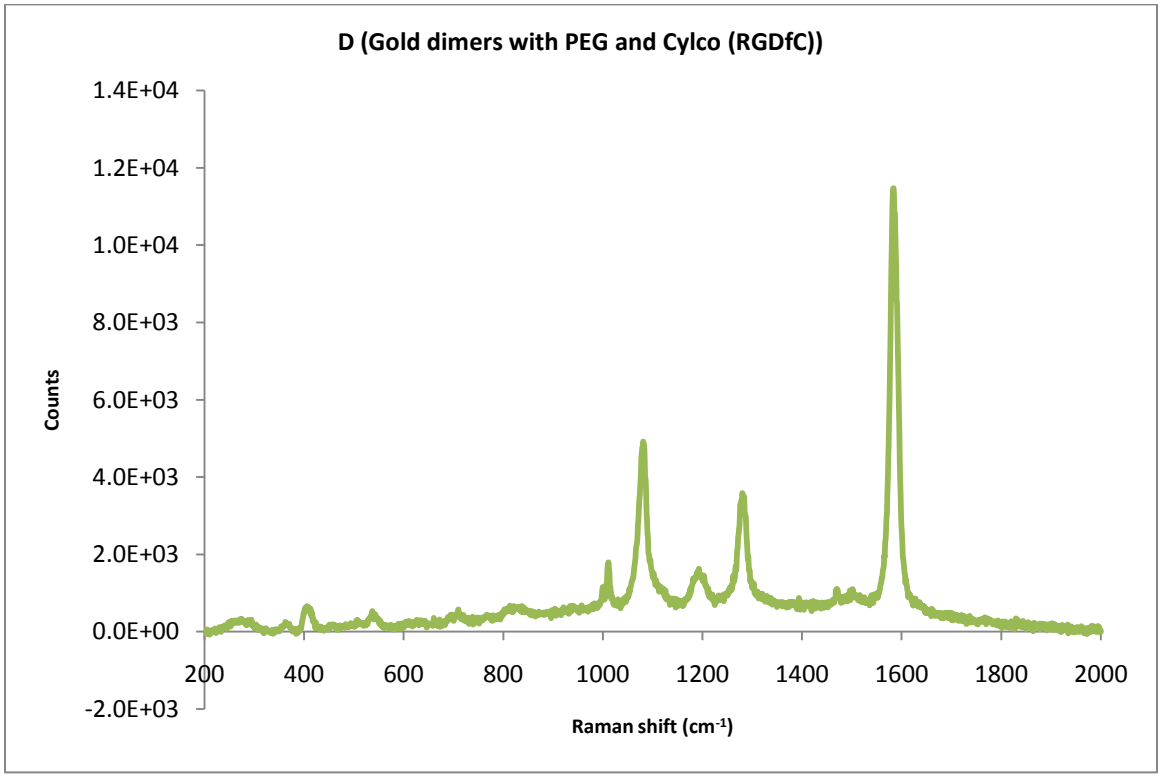

Figure 26: Raman spectrum of sample D.

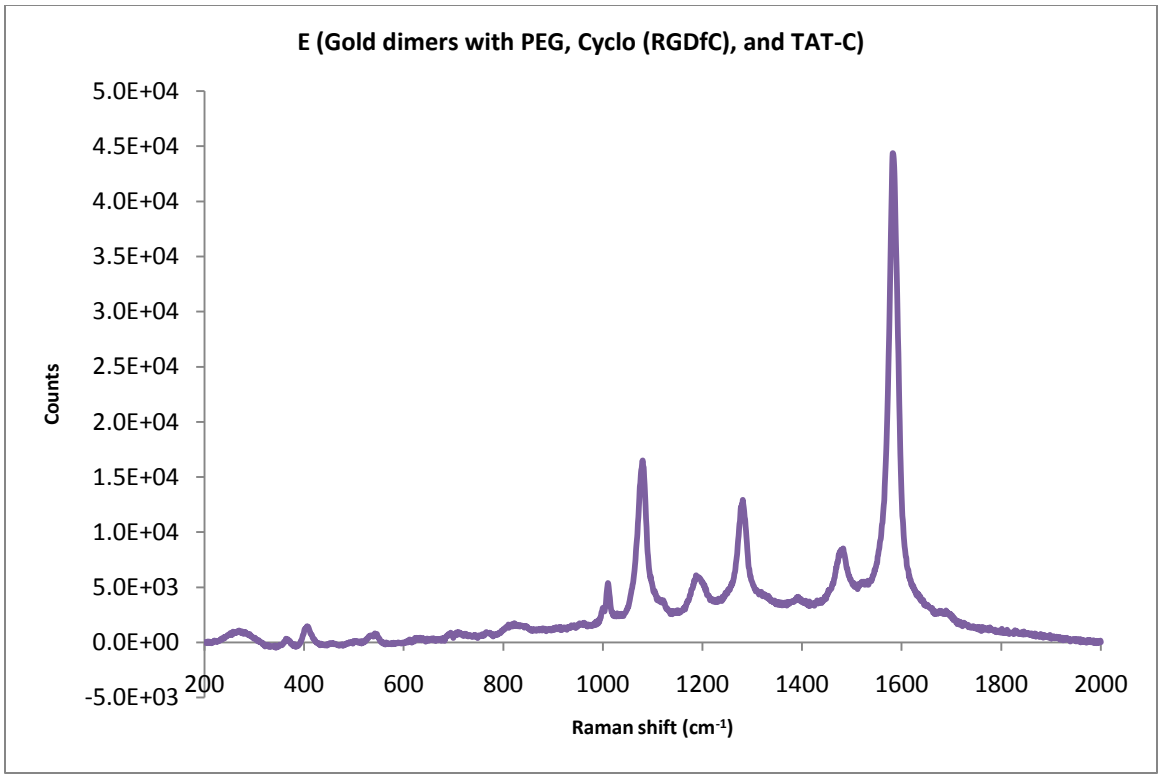

Figure 27: Raman spectrum of sample E.

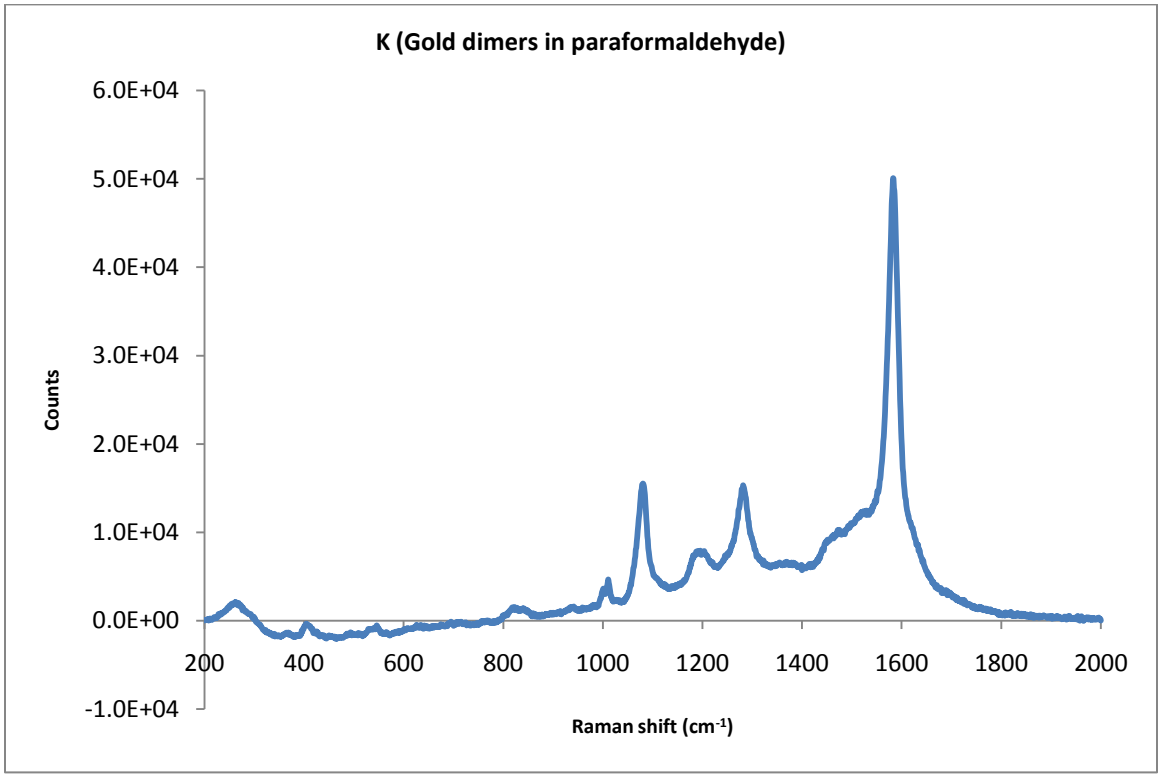

Figure 28: Raman spectrum of sample K.

5.3.3. Transmission Electron Microscopy (TEM)

TEM micrographs of sample E confirmed the formation of dimers and trimers (figs. 29 through 31). A histogram of the type of nanoparticle structure showed a prevalence of dimers (fig. 32). The micrographs were obtained 2 days after synthesis. The addition of PEG and peptides prevented the agglomeration of the particles during that time.

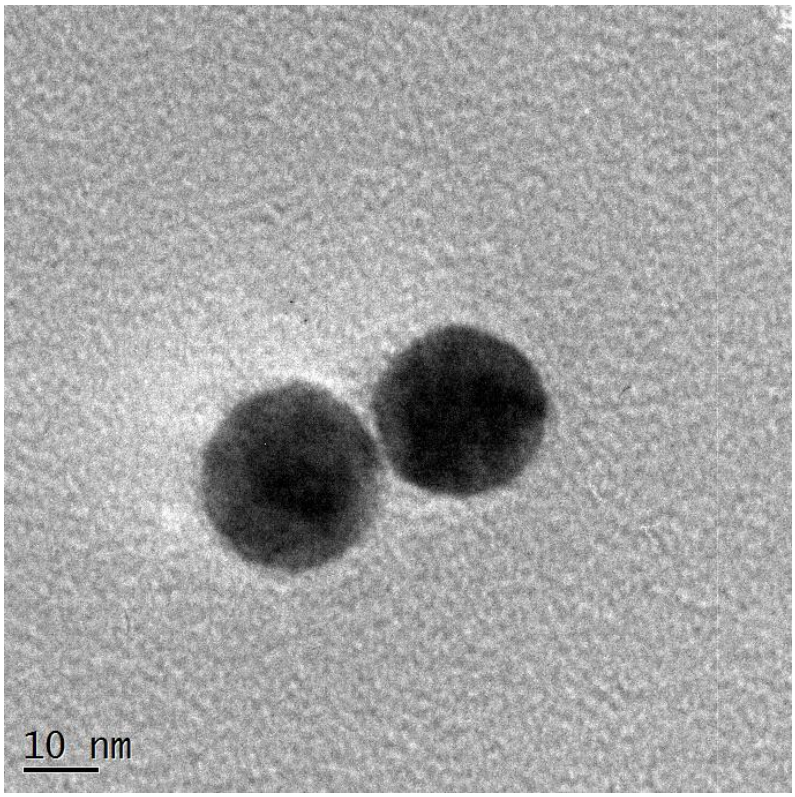

Figure 29: TEM micrograph of gold nanoparticle dimer functionalized with PEG and peptides.

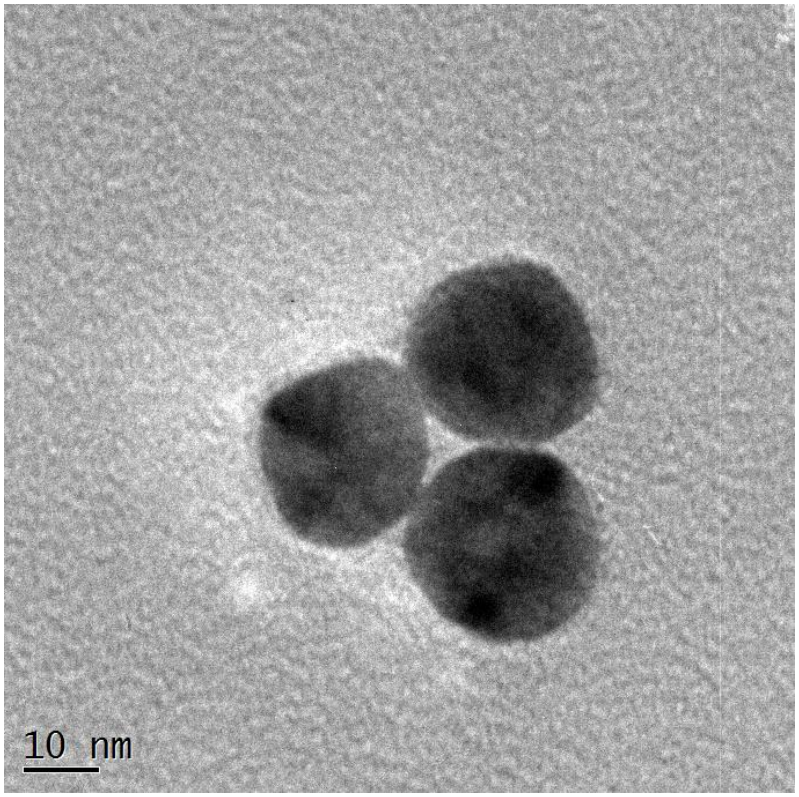

Figure 30: TEM micrograph of gold nanoparticle trimer functionalized with PEG and peptides.

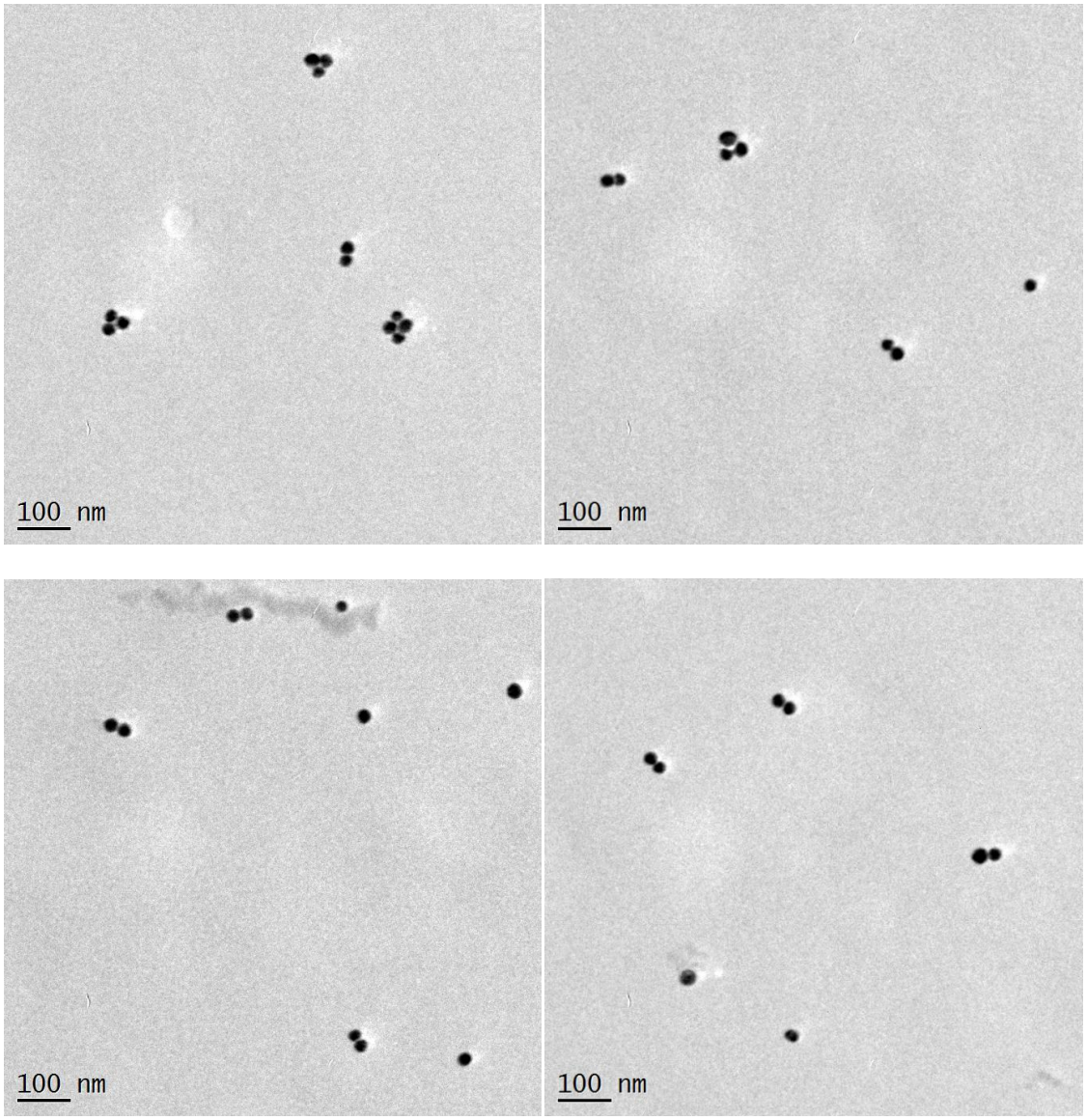

Figure 31: TEM micrographs of gold nanoparticle monomers, dimers, trimers, and quadmers functionalized with PEG and peptides.

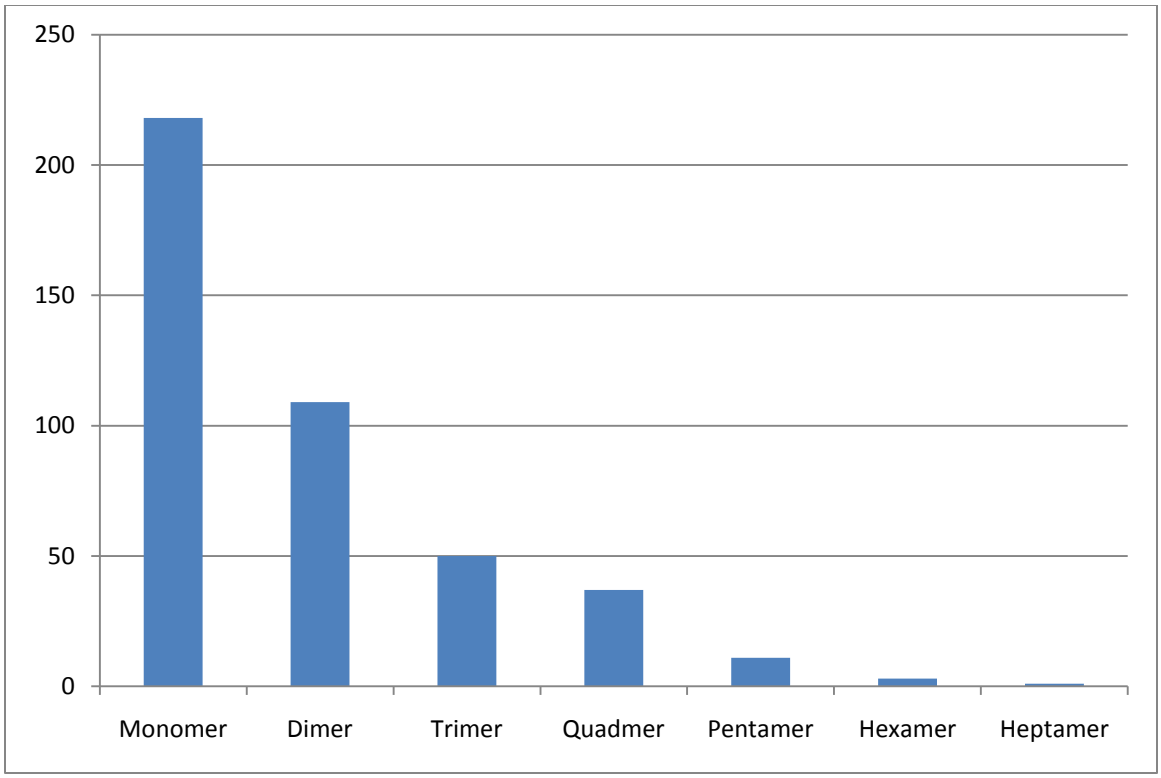

Figure 32: Histogram of the assembly size distribution.

5.4. Stability of Functionalized Nanoparticles

The addition of 1x PBS to samples A through G gave indication as to how stable the particles would be in presence of a physiological solution. Immediately after adding the PBS, suspensions A, B, and G turned grey then clear as the nanoparticles flocculated and fell out of solution. Sample F slowly turned a purple/grey color, but was sufficient for obtaining absorption spectra. The PEG-functionalized nanoparticles, C, D, and E, maintained their orange/red color. This is expected as the PBS changed the ionic strength of the solution and those particles that were not sterically stabilized flocculated. UV-Vis shows no change in the plasmon peaks of C, D, and E indicative of a stable solution (fig. 33). F shows a significant decrease in the plasmon peak and the growth of a second

plasmon band in the 600 nm to 700 nm range indicating the beginning of flocculation.

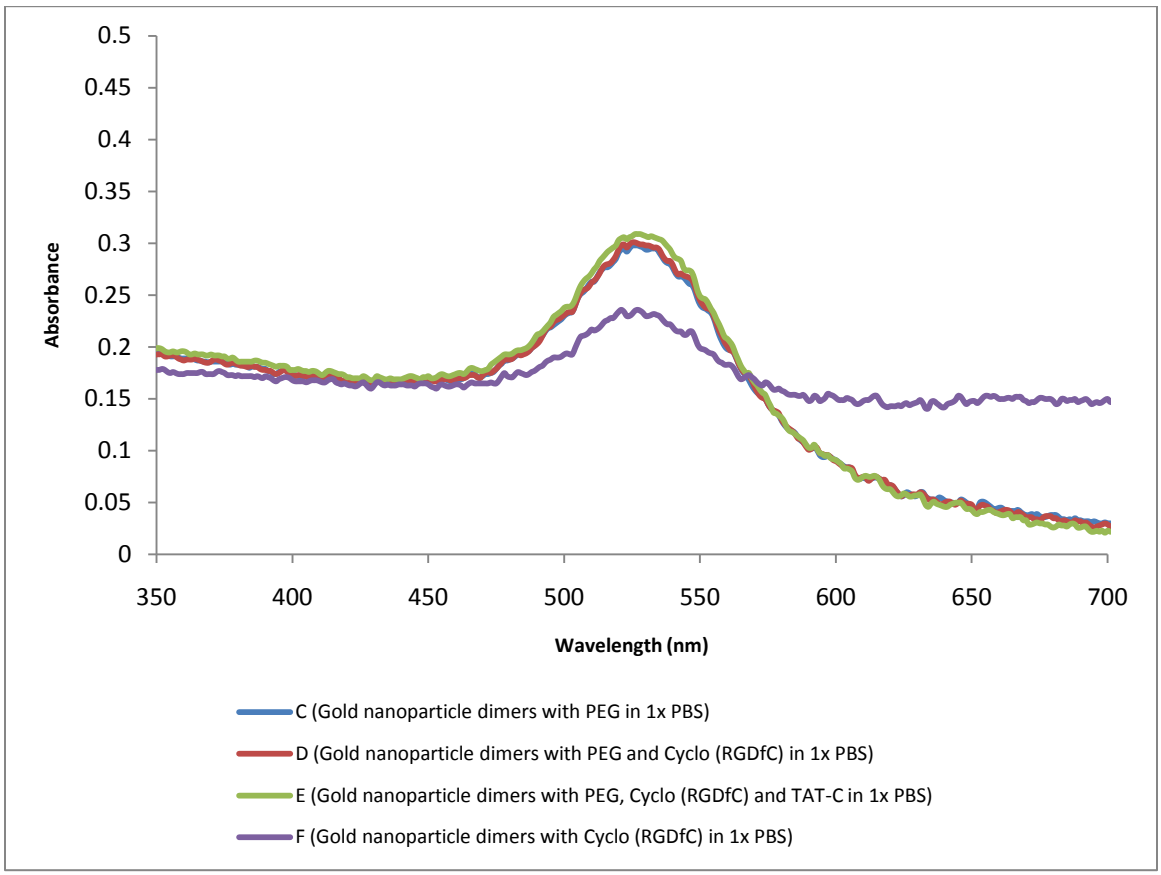

Figure 33: Absorption spectra of gold nanoparticle dimers suspended in 1x PBS.

The addition of the cell culture medium to C, D, and E and the subsequent washing out was used to determine if the proteins and chemicals in the media affected the structure of the PEG protected nanoparticles. UV-Vis spectra showed no significant shift of the SPR peak and no growth of any secondary plasmons (fig. 34). Because of the inert properties of PEG, no significant adsorption on the PEG protected nanoparticles occurred.

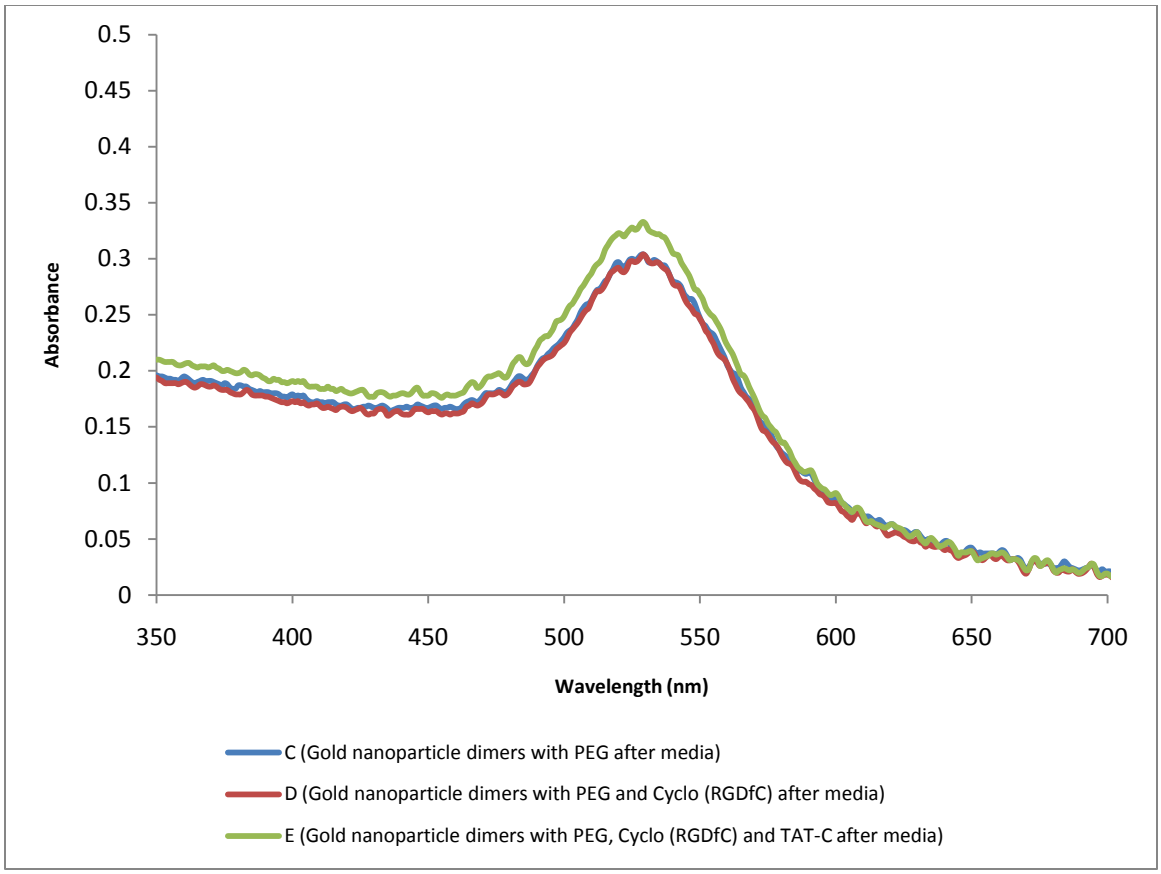

Figure 34: Absorption spectra of gold nanoparticle dimers after suspension in media.

5.5. Characterization of U87 Cells

5.5.1. Fluorescence Microscopy:

In using a fluorescently labeled surfactant to indicate the location of a particle, there is some concern that any remaining unbound surfactants can give false indications. For example, a FITC signal coincident with the U87 cells may be either the result of adsorption or endocytosis of the FITC labeled nanoparticles or the result of unbound FITC-PEG molecules adsorbing to the cells. An excessive amount of unbound FITC-PEG molecules, more molecules than those added to the gold nanoparticle solutions, was added to the U87 cells

to see if any interaction occurred. Fluorescence microscopy of the cells did not show any FITC signal indicating the FITC-PEG molecules were washed out during the fixing steps. Therefore, unbound FITC-PEG do not adsorb or undergo endocytosis into U87 cells and any FITC signal observed would be indicative of the location of FITC labeled nanoparticles.

Fluorescence microscopy of samples C_1, D_1, E_1 at a laser power of 25% showed a green FITC signal coincident with the U87 cells (figs. 35 through 37). The nucleus of the cells can be seen by the blue fluorescence of DAPI. The coincidence proves that the nanoparticles are either adsorbed to the cell membrane or inside the cell.

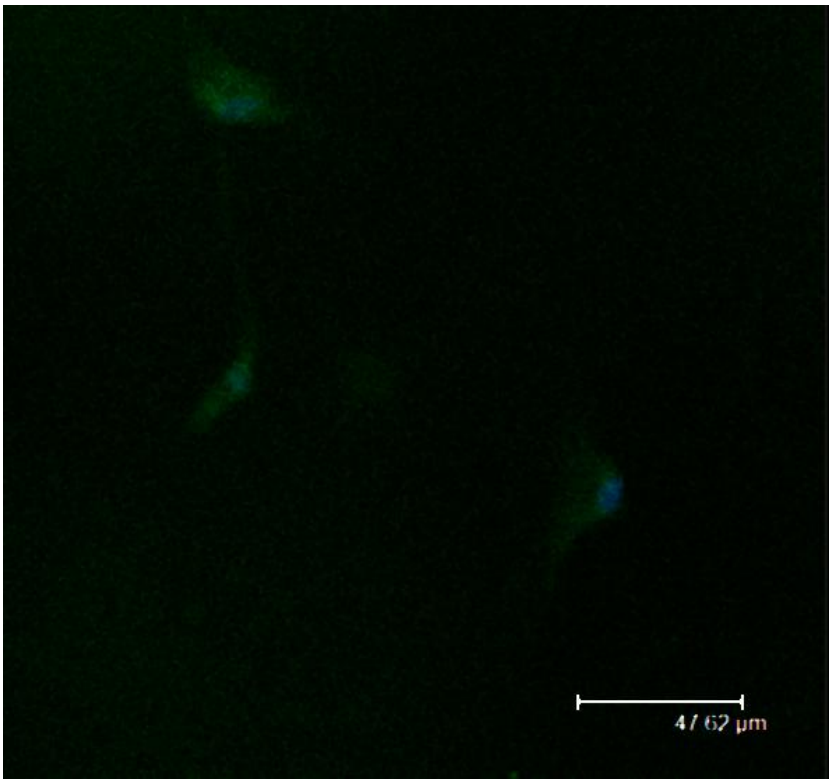

Figure 35: Fluorescence microscopy image of U87 cells with labeled gold nanoparticle dimers, C_1.

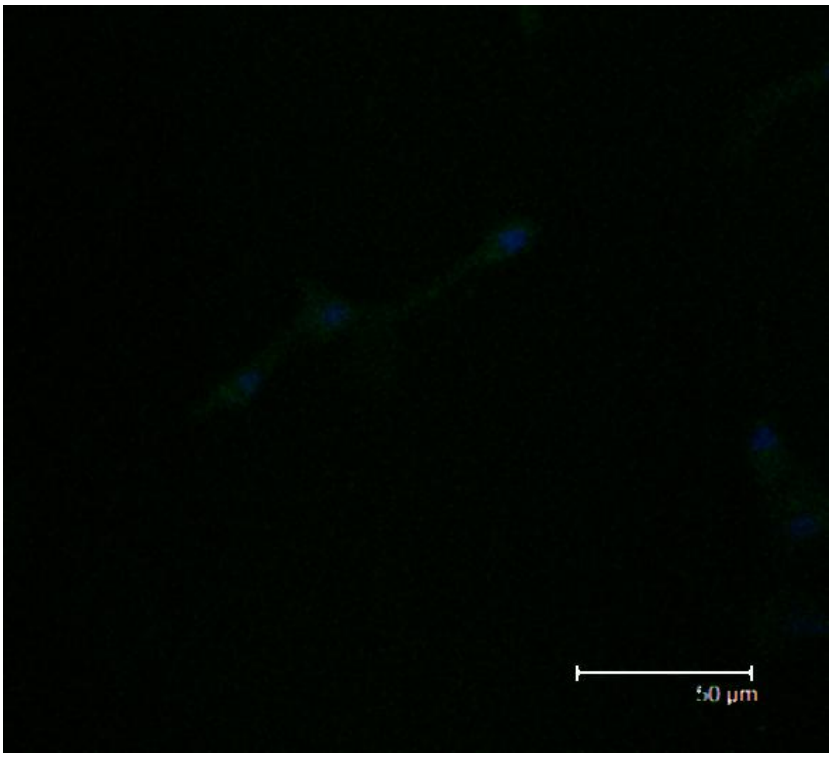

Figure 36: Fluorescence microscopy image of U87 cells with labeled gold nanoparticle dimers, D_1.

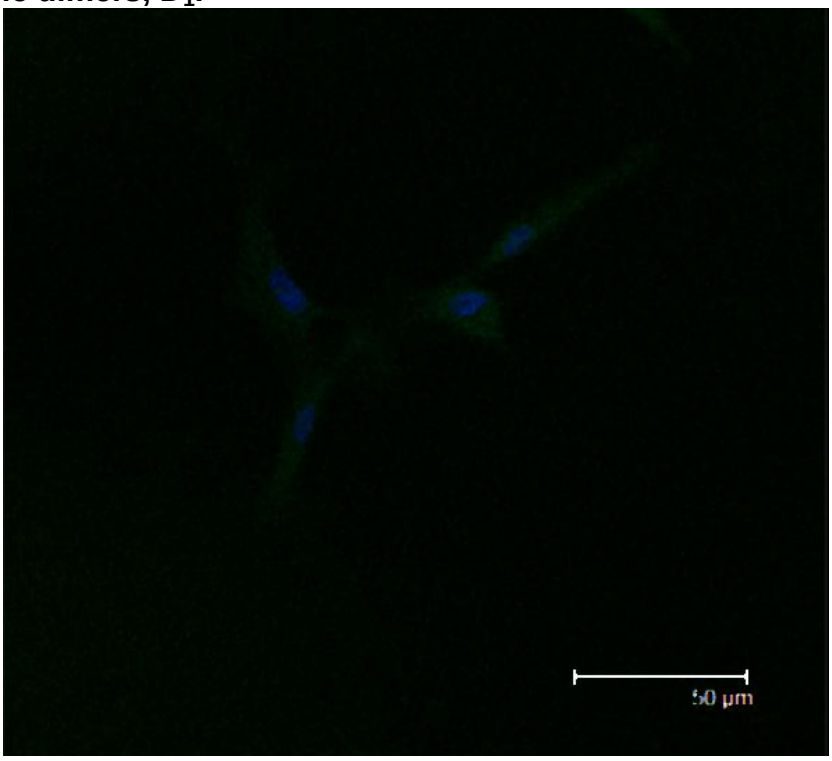

Figure 37: Fluorescence microscopy image of U87 cells with labeled gold nanoparticle dimers, E_1.

To determine if the nanoparticles are inside the cell or only adsorbed to the cell membrane, trypan blue was added to quench any FITC signal outside the cell. In the case of the nanoparticles with PEG-only, C_1, all of the FITC signal was quenched indicating that nonspecific adsorption had taken place (fig. 36). The nanoparticles that included Cyclo (RGDfC), D_1, showed a very slight amount of FITC fluorescence at 50% power (fig. 36). The nanoparticles that included both Cyclo (RGDfC) and TAT-C showed a clear amount of FITC fluorescence at 50% power (fig. 38). This leads to the conclusion that the Cyclo (RGDfC) peptide increased the amount of nanoparticles adsorbed to the cell membranes and led to an increased probability of particle endocytosis. The addition of the TAT-C peptide led to a significant increase in the probability of particle endocytosis.

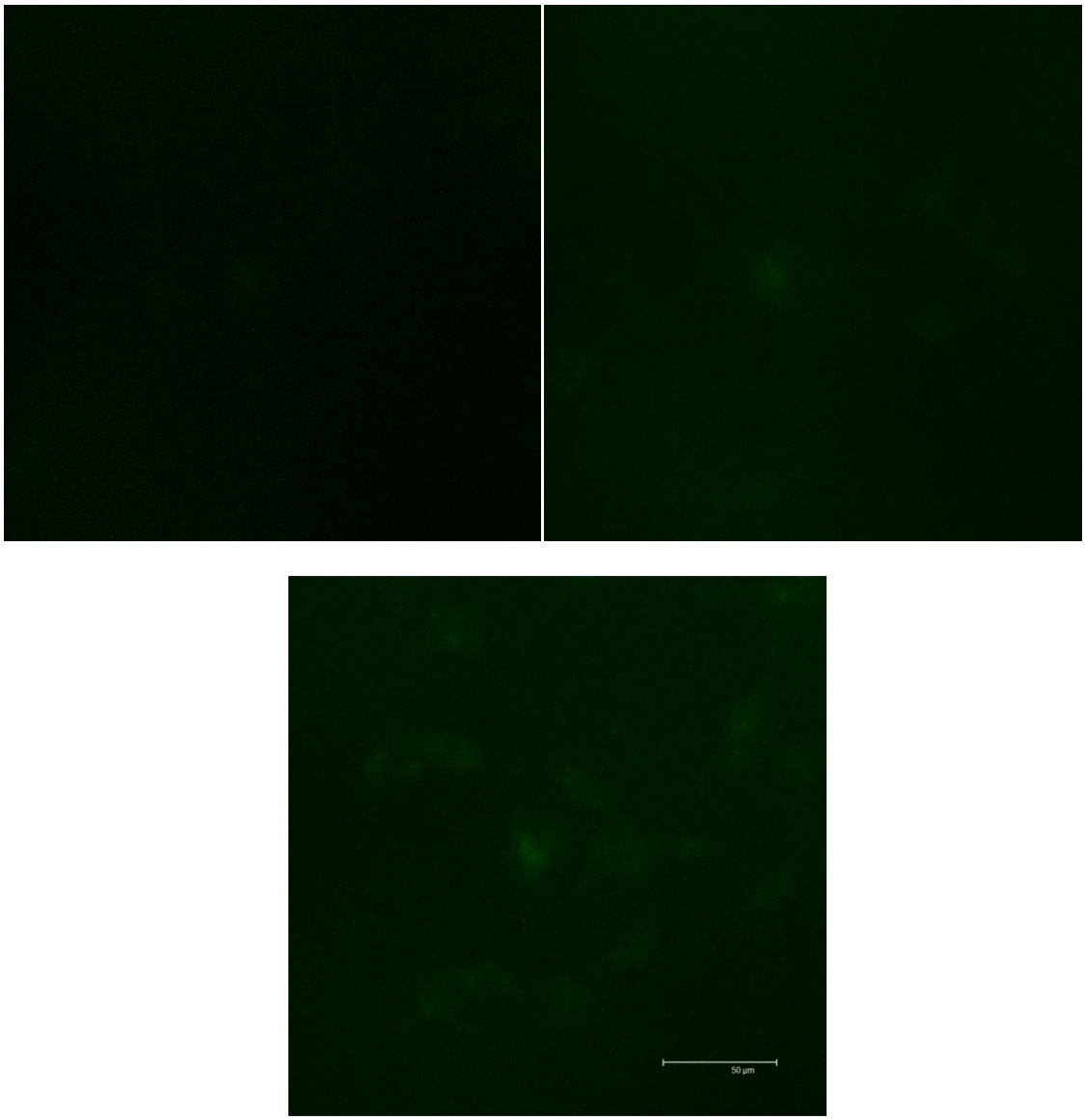

Figure 38: Fluorescence microscopy images of C_1, D_1 and E_1 after the addition of trypan blue.

5.5.2. Raman Spectroscopy:

The addition of trypan blue caused the Raman signals of C_1, D_1, and E_1 to be supersaturated. Therefore, samples C_2, D_2, and E_2 were prepared in the same manner as the first Petri dishes and characterized using Raman spectroscopy. The lens used for scanning was a 50x dry lens with a short working distance.

Future work will incorporate immersive lens with higher magnification allowing for better detection of the Raman signals.

As an effect of the drying, the gold nanoparticles began to aggregate to the point of gold clusters being visible under the microscope. The degree of gold on the cells gave some information on the relative amounts of gold in the cells. Most of the cells in sample C_2 did not have gold particles (fig. 39), and only rarely a cell was found to include nanoparticles (fig. 40). On the other hand, samples D_2 (fig. 41) and E_2 (fig. 42) had a higher number of cells with gold particles. This further supports the conclusion that the Cyclo (RGDfC) increased cell membrane attachment while the majority of PEG-only nanoparticles were washed away during the fixing steps.

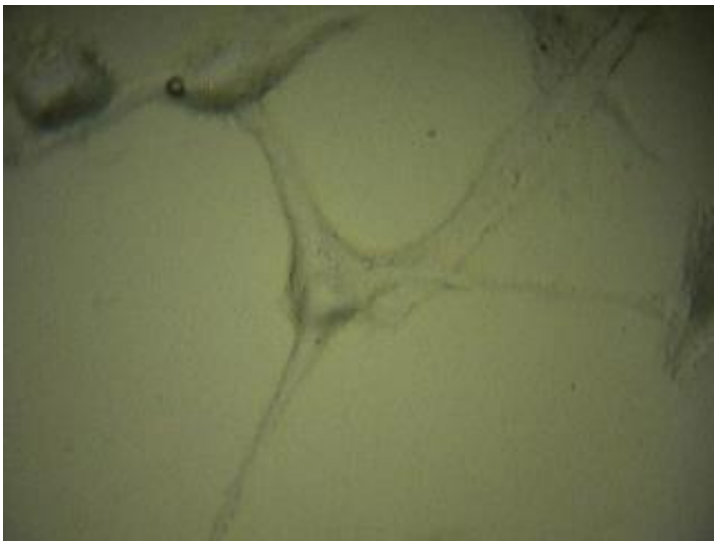

Figure 39: Common C_2 cell without gold particles.

Figure 40: Rare C_2 cell with gold particles.

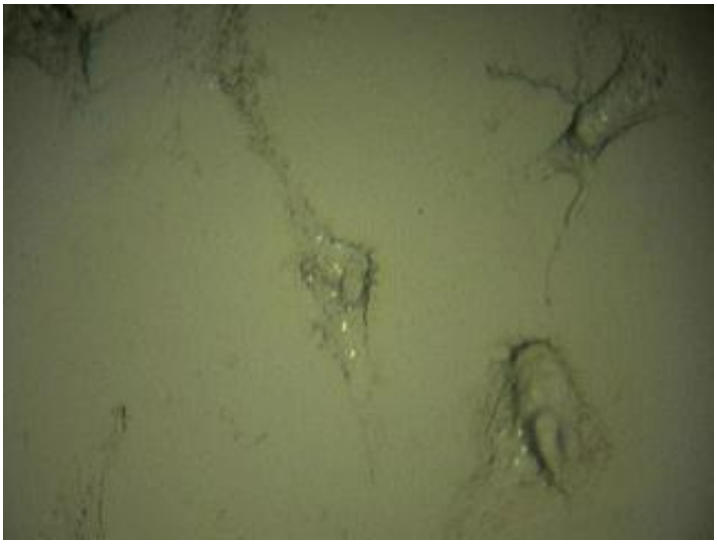

Figure 41: Common D_2 cell with gold particles.

Figure 42: Common E_2 cell with gold particles.

The cells were scanned at 100% power with a 50 mW 633 nm laser. There were no DBDT SERS signals from any of the cells in C_2 and D_2 despite multiple scans. However, by point targeting random locations within the cells of E_2, DBDT SERS signals were able to be found (figs. 43 and 44). The peaks in E_2 matched the peaks observed in the dried out version of sample E (fig. 26). No peaks were observed in scanning the areas outside the cells. One week after the fixing of the cells, E_2 was scanned again. A DBDT SERS signal was still detectable inside the cells.

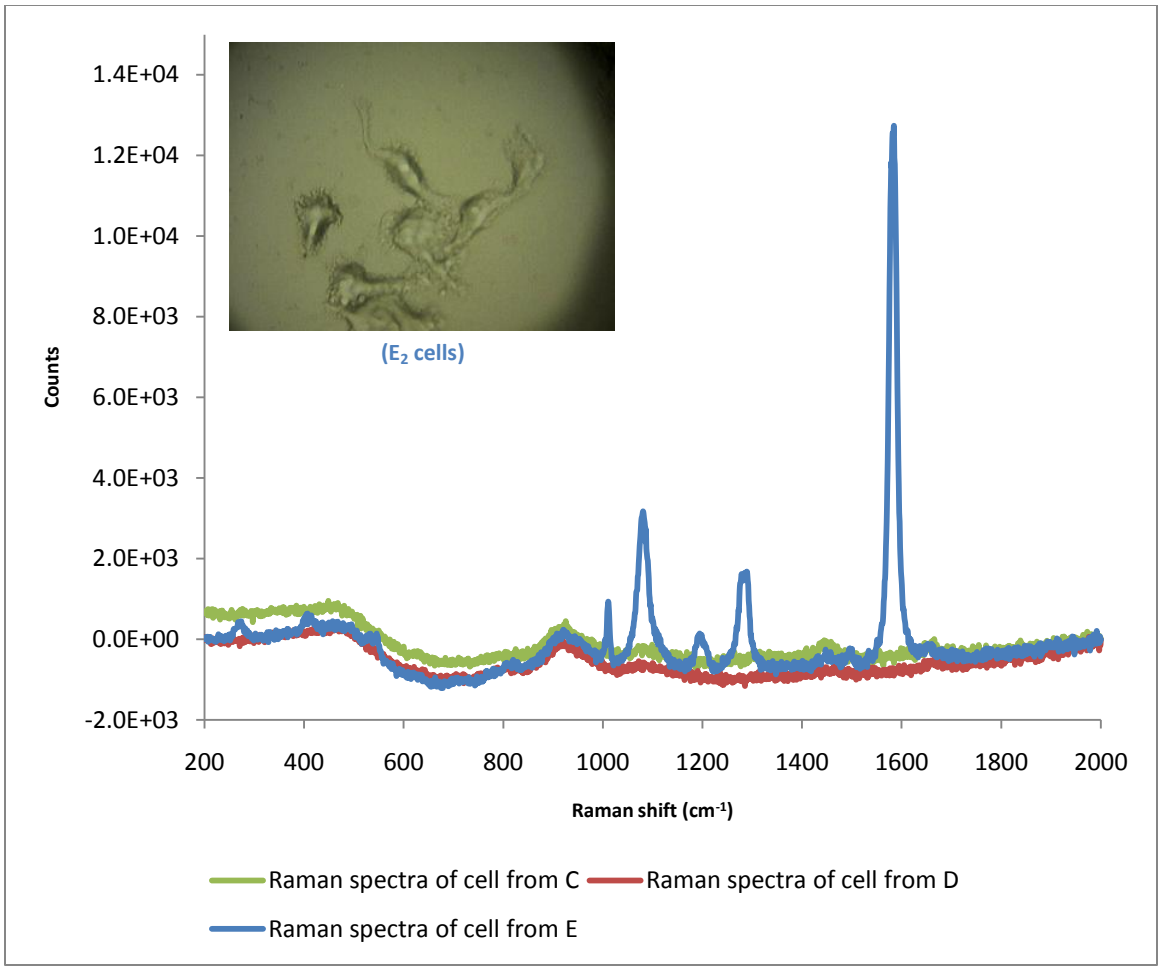

Figure 43: Raman spectra of C_2, D_2, and E_2 cells.

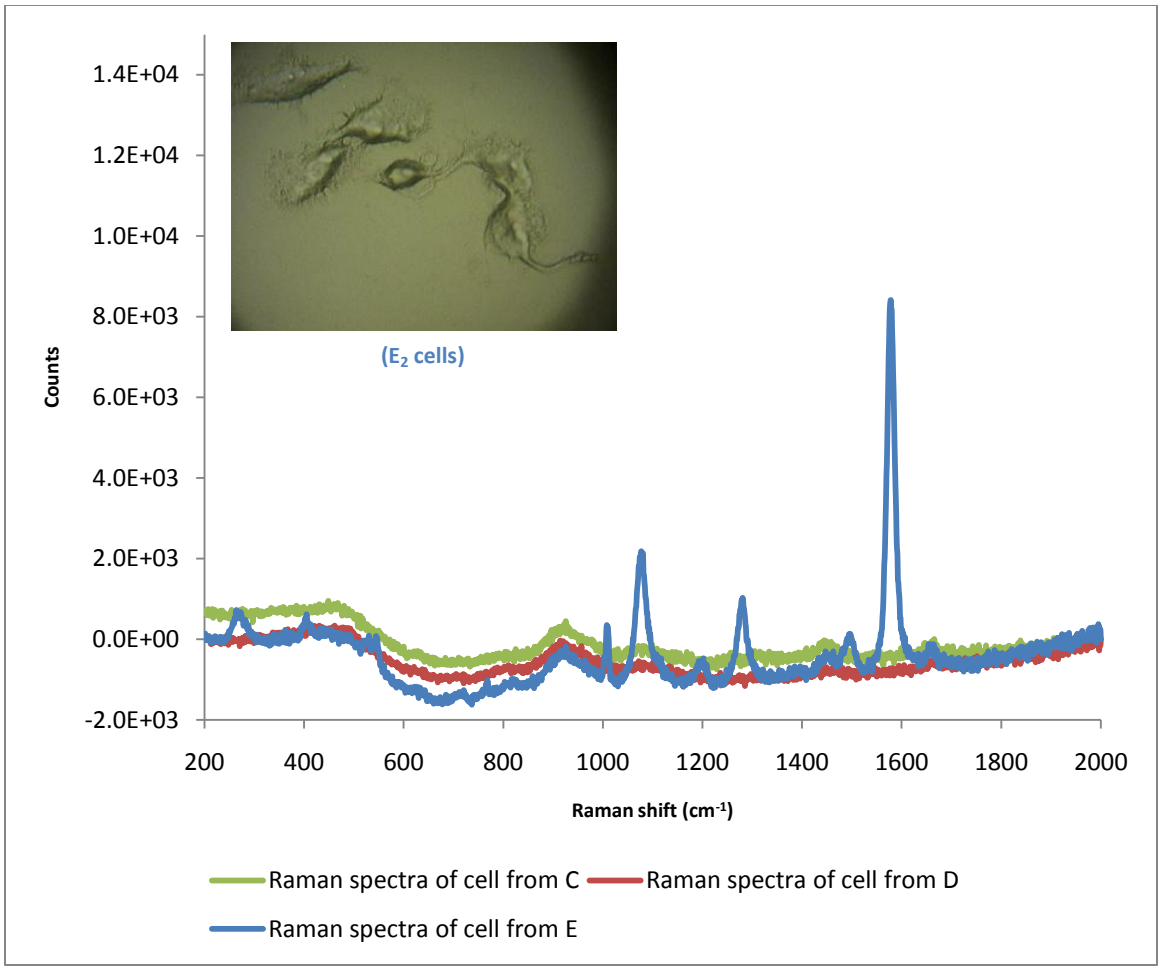

Figure 44: Additional Raman spectra of C_2, D_2, and E_2 cells.

6. DISCUSSION

The synthesis of nanoparticle-based imaging and drug delivery system is a complex task that requires the knowledge of many aspects concerning not only the nanomaterial synthesis and stability, but also its interaction with the biological systems and its optimization in relationship to the proposed transduction mechanism. In this thesis I have reported on the development of gold nanoparticle-based systems that are not only extremely Raman active, due to the surface enhanced Raman scattering effect, but are also stable in the biological environment and capable of efficiently penetrating U87 human glioblastoma cells. In addition to the above, this system has shown the ability of giving rise to an intense SERS signal originating intracellularly, opening new routes to the use of SERS-active nanoparticle-based systems for cancer cell detection. To achieve this success, this project has required the understanding and the analysis of many different issues, from the synthesis of the nanoparticles to the evaluation of cellular uptake.

First of all, the citrate reduction of the gold salt provided a monodispersed solution of gold nanospheres suitable for dimerization and functionalization. Typically, depositing a drop of this solution on a TEM grid will lead to particle agglomeration as a consequence of drying. Therefore, a small sample of the gold nanospheres was functionalized with BSPP to create a strong negative charge on the surface of the particles. The repelling force on the surfaces led to a more dispersed arrangement of nanospheres on the grid. As a result, an accurate particle size was obtained which also allowed the calculation of an

extinction coefficient. The sample concentration was then determined using the Beer-Lambert law and the data collected using the UV-Vis spectrophotometer.

Due to the insolubility of DBDT in water, the dimerization reaction needed to incorporate a new solvent in a two-phase system, where DBDT was extracted to the aqueous phase driven by the high affinity of thiols for gold. Comparison of gold nanoparticles absorption spectra showed no significant changes before and after the addition of THF. Therefore, THF was found to be a suitable alternative for the addition of DBDT.

DBDT adsorption was confirmed by a red shifting of the nanoparticle's SPR. The higher the molar ratio of DBDT, the further the red-shift of the plasmon band, indicative of the formation of nanoparticle aggregates. Due to the chemical structure of DBDT, the nanoparticle aggregation would continue to proceed in the absence of a stabilizing molecule: therefore, PEG was used to quench the aggregation, also in view of its antifouling and biocompatibility properties.

Via addition of stabilizers, the assembly of the particles was limited to dimers, trimers, and small aggregates. The higher affinity of longer thiols over shorter thiols leads to a place exchange. However due to steric hindrance reasons, the DBDT at the junctions is not replaced and is able to keep the nanoparticles in their original assembly. The adsorption of the surfactants led to an expected change in the effective hydrodynamic diameter. TEM micrographs of the PEG/peptide-capped nanoparticles confirmed that the assembly was limited to dimers, trimers and small aggregates.

The DBDT molecules located in the junctions between two particles were able to give rise to a significantly enhanced Raman signal owing to the SERS effect. The presence of a SERS effect was determined by comparing the DBDT peak pattern obtained with and without nanoparticles, evidenced in the selective enhancement of only specific peaks.

The addition of PEG was necessary to prevent flocculation of the nanoparticle dimers in the presence of buffer. This type of stabilization is critical to avoid coalescence in physiological solutions. The lack of any changes in the SPR of the PEG/peptide dimers when added to PBS, cell culture media, and paraformaldehyde indicated the suitability of the dimers for *in vitro* studies.

Adding a FITC-labeled thiolated PEG within the surface monolayer provided a method for observing with a traditional approach (i.e. fluorescence microscopy) the location of the dimers after their addition to the U87 cells. The overlay of the FITC signal with the cell structure in all cases indicated that nonspecific adhesion occurs with or without the targeting peptide Cyclo (RGDfC). However, the quenching of FITC outside the cell membrane observed using trypan blue shows that the degree of cellular uptake significantly decreases without Cyclo (RGDfC) or TAT-C. This was further confirmed by the increased amount of small, observable aggregated particles in samples D and E with Cyclo (RGDfC) and TAT-C functionalized dimers, relative to the cells in sample C with the PEG only dimers. The Cyclo (RGDfC) peptide likely increased the rate of cellular adhesion leading to an increase in receptor-mediated endocytosis. This can be seen by the increase in the FITC signal intensity for sample D relative to C, after trypan

blue treatment. The higher intensity of FITC in E relative to D, post addition of trypan blue, indicates an increased degree of endocytosis with the incorporation of the cell penetrating peptide, TAT-C.

The SERS signal obtained in the cells incubated with Cyclo (RGDfC) and TAT-C functionalized dimers confirms the validity of Raman-active nanoparticle tags for optical detection. Furthermore, the stability of the approach is confirmed by the ability of obtaining a SERS signal a week after treating the cells with the nanoparticle-based tags.

There is some question as to why there is no SERS signal originating from the nanoparticles without TAT-C. Fluorescence microscopy shows the extracellular adsorption of the PEG-only dimers and both extracellular adsorption and intracellular uptake of the Cyclo (RGDfC) particles. Yet, despite multiple scans, no SERS signal can be detected. Future work that incorporates Raman spectroscopy with higher magnification- and water immersion-lenses may help in unraveling this issue.

7. CONCLUSION

The nanoparticle dimers described in this thesis demonstrated the ability to target and penetrate glioblastoma cells and to subsequently produce an observable signal when scanned with a Raman spectrometer. These results validate the use of Raman-active nanoparticle systems for targeting and detecting glioblastoma cells *in vitro*. Additionally, the nanoparticle system reinforces the applicability of using Raman reporters for biosensing. Unlike fluorescent dyes, the Raman signal does not decay over time as a result of photobleaching. Due to the specific peak patterns of Raman reporters, multiple nanoparticle-based systems can be used at any one time simply by interchanging and multiplexing the linker. While this work only used DBDT, the linker can be easily interchanged with a range of dithiolated molecules.

The addition of PEG ensured that the nanoparticles were stable in biological media *in vitro,* however future experiments will be required to validate the stability and efficiency of the nanoparticles *in vivo*. Additionally, in vivo studies can be used to validate the ability of the nanoparticles to cross the blood brain barrier.

This work incorporated both a targeting peptide and a peptide known to facilitate endocytosis. However, the functionalization is not limited to Cyclo (RGDfC) nor TAT-C. By using the correct molar ratios of PEG and peptides, these nanoparticles can be functionalized to target any desired objective. Many thiolated peptides are commercially available, and the ease at which a thiolated

peptide can adsorb to a gold nanoparticle ensures that these nanoparticles can be designed with a whole range of applications in mind.

To further validate the system as a cell sensor, multiple cell lines should be incorporated. A variety of nanoparticles functionalized with different targeting peptides, each dimerized with a unique linker molecule, can be added to a complex of cells. Theoretically, each type of nanoparticle would preferably undergo endocytosis into their targeted cells. With the specificity of the SERS Raman signal, each type of cell can therefore be distinguishable.

While this works sets a foundation for Raman based sensing and mapping, future work in this field can also apply toward drug delivery. During the additions of the PEG and peptides, a thiolated surfactant functionalized with a therapeutic drug can be incorporated. This surfactant would need to incorporate a drug releasing mechanism that exploits a property change that occurs once inside the cell. An example of such a change might be the drop in pH inside an endosome [72].

While doctors and patients continue the fight against cancer every day, they are limited by the tools and technology available to them. In this regard, Raman-based nanoparticle systems are an important tool in the fields of biotechnology and nanomedicine. They have the potential to provide accurate *in vivo* diagnostic information critical to therapeutics. Their versatility sets the ground work for future nanosized drug delivery systems which avoid the detrimental side effects of today's chemotherapeutics.

REFERENCES

1. *Cancer Facts & Figures.* American Cancer Society, 2010.

2. J. P. Tian, A.F., J. Wang, and E. A. Chiocca, *Modeling the effects of resection, radiation and chemotherapy in glioblastoma.* Journal of Neurooncology, 2009. **91**: p. 287-293.

3. P. R. Lockman, R.J.M., M. A. Khan, and D. D. Allen, *Nanoparticle Technology for Drug Delivery Across the Blood-Brain Barrier.* Drug Development and Industrial Pharmacy, 2002. **28**: p. 1-13.

4. G. Sonavane, K.T., and K. Makino, *Biodistribution of colloidal gold nanoparticles after intravenous administration: Effect of particle size.* Colloids and Surfaces B: Biointerfaces, 2008. **66**(2): p. 274-280.

5. M. E. Davis, Z.G.C.a.D.M.S., *Nanoparticle therapeutics: an emerging treatment modality for cancer.* Nature Reviews, 2008. **7**: p. 771-782.

6. T-Y. Liu, S.-H.H., D-M. Liu, S-Y. Chen, and I-W. Chen, *Biomedical nanoparticle carriers with combined thermal and magnetic responses.* Nano Today, 2009. **4**: p. 52-65.

7. W. Yang, P.T., J. J. Gooding, S. P. Ringer and F. Braet, *Carbon nanotubes for biological and biomedical applications.* Nanotechnology, 2007. **18**: p. 1-12.

8. M. Slevin, L.B., M. Grau-Olivares, M. Ramis, J. Sendra, M. Morrison and J. Krupinski, *Combining nanotechnology with current biomedical knowledge for the vascular imaging and treatment of atherosclerosis.* Molecular BioSystems, 2010. **6**: p. 444–45.

9. C. L. Gladson, D.A.C., *Glioblastoma expression of vitronectin and the alpha v beta 3 integrin. Adhesion mechanism for transformed glial cells.* The Journal of Clinical Investigation, 1991. **88**(6): p. 1924–1932.

10. S. Vemuri, C.T.R., *Preparation and characterization of liposomes as therapeutic delivery systems: a review.* Pharmaceutica Acta Helvetiae, 1995. **70**(2): p. 95-111.

11. Dykes, G.M., *Dendrimers: a review of their appeal and applications.* Journal of Chemical Technology & Biotechnology, 2001. **76**(9): p. 903–918.

12. S. Bisht, G.F., J-B. M.Koorstra, M. Mullendore, H. Alvarez, C. Karikari, M. A.Rudek, C. K.Lee, A. Maitra, and A. Maitra, *In vivo characterization of a*

polymeric nanoparticle platform with potential oral drug delivery capabilities. Molecular Cancer Therapeutics, 2008. **7**(12): p. 3878-3888.

13. T. P. Thomas, R.S., A. Kotlyar, J.Kukowska-Latallo, and J. R. Baker Jr, *Dendrimer-based tumor cell targeting of fibroblast growth factor-1.* Bioorganic & Medicinal Chemistry Letters, 2010. **20**(2): p. 700-703.

14. A. R. Menjoge, R.M.K., and D. A. Tomalia, *Dendrimer-based drug and imaging conjugates: design considerations for nanomedical applications.* Drug Discovery Today, 2010. **15**(5-6): p. 171-185.

15. K. Hettiarachchi, A.P.L., *Polymer–lipid microbubbles for biosensing and the formation of porous structures.* Journal of Colloid and Interface Science, 2010. **344**: p. 521-527.

16. N. Y. Rapoport, A.M.K., J. E. Shea, C. L. Scaife, and K-H. Nam, *Controlled and targeted tumor chemotherapy by ultrasound-activated nanoemulsions/microbubbles.* Journal of Controlled Release, 2009. **138**(3): p. 268-276.

17. E. C. Le Ru, P.G.E., *Principles of Surface-Enhanced Raman Spectroscopy*. 2009, Elsevier: Amsterdam.

18. F. E. Wagner, S.H., L. Stievano, S. Calogero, Q. A. Pankhurst, and K. -P. Martinek, *Before striking gold in gold-ruby glass.* Nature, 2000. **407**: p. 691-692.

19. G. Padeletti, P.F., *How the masters in Umbria, Italy, generated and used nanoparticles in art fabrication during the Renaissance period.* Applied Physics A, 2003. **76**: p. 515-525.

20. P. P. Edwards, J.M.T., *Gold in a Metallic Divided State—From Faraday to Present-Day Nanoscience.* Angewandte Chemie, 2007. **46**: p. 5480 – 5486.

21. M. De, P.S.G., and V. M. Rotello, *Applications of Nanoparticles in Biology.* Advanced Materials, 2008. **20**: p. 1-17.

22. B. Nikoobakht, M.A.E.-S., *Preparation and Growth Mechanism of Gold Nanorods (NRs) Using Seed-Mediated Growth Method.* Chemical Materials, 2003. **15**: p. 1957-1962.

23. H. Wang, C.X., R. Chen, and W. D. Zhang, *Fabrication and Growth Mechanism of Star-shaped Gold nanoparticles via seed-Mediated Growth Method.* Advanced Materials Research, 2010. **152**: p. 600-604.

24. C-J. Huang, Y.-H.W., P-H. Chiu, M-C. Shih, and T-H. Meen, *Electrochemical synthesis of gold nanocubes.* Materials Letters, 2006. **60**: p. 1896-1900.

25. J. Turkevich, P.C.S.a.J.H., *A Study of the Nucleation and Growth Processes in the Synthesis of Colloidal Gold.* Discuss. Faraday Soc.,, 1951. **11**: p. 55-75.

26. S. Kumar, K.S.G., and R. Kumar, *Modeling of Formation of Gold Nanoparticles by Citrate Method.* Industrial & Engineering Chemistry Research, 2007. **46**: p. 3128-3136.

27. M. Brust, M.W., D. Bethell, D. J. Schiffrin and R. Whyman, *Synthesis of Thiol-derivatised Gold Nanoparticles in a Two-phase Liquid-Liquid System.* Journal of Chemical Society, Chemical Communications, 1994: p. 801-802.

28. Mie, G., *Beiträge zur Optik trüber Medien, speziell kolloidaler Metallösungen.* Annalen der Physik, 1908. **330**(3): p. 377-445.

29. K. Lance Kelly, E.C., Lin Lin Zhao, and George C. Schatz, *The Optical Properties of Metal Nanoparticles: The Influence of Size, Shape, and Dielectric Environment.* Journal of Physical Chemistry, 2003. **107**: p. 668-677.

30. P. K. Jain, X.H., I. H. El-Sayed and M. A. El-Sayed, *Review of Some Interesting Surface Plasmon Resonance-enhanced Properties of Noble Metal Nanoparticles and Their Applications to Biosystems.* Plasmonics, 2007. **2**: p. 107-118.

31. Swinehart, D.F., *The Beer-Lambert Law.* Journal of Chemical Education, 1962. **39**(7): p. 333-335.

32. P. K. Jain, K.S.L., I. H. El-Sayed, and M. A. El-Sayed, *Calculated Absorption and Scattering Properties of Gold Nanoparticles of Different Size,Shape, and Composition: Applications in Biological Imaging and Biomedicine.* American Chemical Society, 2006. **110**: p. 7238-7248.

33. S. Link, M.A.E.-S., *Size and Temperature Dependence of the Plasmon Absorption of Colloidal Gold Nanoparticles.* American Chemical Society, 1999. **103**(21): p. 4212-4217.

34. X. Liu, M.A., J. Wang, Q. Huo, *Extinction coefficient of gold nanoparticles with different sizes and different capping ligands.* Colloids and Surfaces B: Biointerfaces, 2007. **58**: p. 3–7.

35. I. H. El-Sayed, X.H., and M. A. El-Sayed, *Surface Plasmon Resonance Scattering and Absorption of anti-EGFR Antibody Conjugated Gold Nanoparticles in Cancer Diagnostics: Applications in Oral Cancer.* Nano Letters, 2005. **5**(5): p. 829-834.

36. C. A. Mirkin, R.L.L., R. C. Mucic, and J. J. Storhoff, *A DNA-based method for rationally assembling nanoparticles into macroscopic materials.* Nature, 1996. **382**: p. 607-609.

37. Singh, R., *C. V. Raman and the Discovery of the Raman Effect.* Physics in Perspective, 2002. **4**: p. 399-420.

38. M. Fleischman, P.J.H., and A. J. McQuillan, *Raman spectra of pyridine adsorbed at a silver electrode.* Chemical Physics Letters, 1974. **26**(2): p. 163-166.

39. J. R. Lombardi, R.L.B., T.Lu, and J. Xu, *Charge-transfer theory of surface enhanced Raman spectroscopy: Herzberg-Teller contributions.* Journal of Chemical Physics, 1986. **8**.

40. H. Xu, E.J.B., M. Käll, and L. Börjesson, *Spectroscopy of Single Hemoglobin Molecules by Surface Enhanced Raman Scattering.* Physical Review Letters, 1999. **83**(21): p. 4357-4360.

41. S. S. Acimovic, M.P.K., M. U. González, and R. Quidant, *Plasmon Near-Field Coupling in Metal Dimers as a Step toward Single-Molecule Sensing.* ACS Nano, 2009: p. 1231–1237.

42. M. Gellner, K.K.a.S.S., *Multiplexing with SERS labels using mixed SAMs of Raman reporter molecule.* Analytical and Bioanalytical Chemistry, 2009. **394**(7): p. 1839-1844.

43. W. Azzam, B.I.W., R. A. Fischer, A. Terfort, and C. Woll, *Bonding and Orientation in Self-Assembled Monolayers of Oligophenyldithiols on Au Substrates.* Langmuir, 2002. **18**: p. 7766-7769.

44. B. Boer, H.M., D. F. Perepichka, J. Zheng, M. M. Frank, Y. J. Chabal, and Z. Bao, *Synthesis and Characterization of Conjugated Mono- and Dithiol Oligomers and Characterization of Their Self-Assembled Monolayers.* Langmuir, 2003. **19**: p. 4272-4284.

45. D. Zanchet, C.M.M., W. J. Parak, D. Gerion, S. C. Williams, and A. P. Alivisatos, *Electrophoretic and Structural Studies of DNA-Directed Au Nanoparticle Groupings.* Journal of Physical Chemistry, 2002. **106**: p. 11758-11763.

46. Turkevich, J., *Colloidal Gold. Part II.* Gold Bulletin, 1985. **18**(4): p. 125-131.

47. S. H. De Paoli Lacerda, J.J.P., C. Meuse, D. Pristinski, M. L. Becker, A. Karim, and J. F. Douglas, *Interaction of Gold Nanoparticles with Common Human Blood Proteins.* ACS Nano, 2010. **4**(1): p. 365-379.

48. S. Ramakrishna, J.M., E. Wintermantelc and Kam W. Leong, *Biomedical applications of polymer-composite materials: a review.* Composites Science and Technology, 2001. **61**(9): p. 1189-1224.

49. L. M. Campos, K.L.K., R. Sakai, J. M. J. Paulusse, D. Damiron, E. Drockenmuller, B. W. Messmore, and and C.J. Hawke, *Development of Thermal and Photochemical Strategies for Thiol−Ene Click Polymer Functionalization.* Macromolecule, 2008. **41**: p. 7063-7070.

50. Zalipsky, S., *Chemistry of polyethylene glycol conjugates with biologically active molecules.* Advanced Drug Delivery Reviews, 1995. **16**(2-3): p. 157-182.

51. J. M. Harris, R.B.C., *Effect of PEGylation on Pharmaceuticals.* Nature, 2003. **2**: p. 214-221.

52. Ulman, A., *Formation and Structure of Self-Assembled Monolayers.* Chemical Reviews, 1996. **96**: p. 1533−1554.

53. Y. Akiyama, H.O., Y. Nagasaki, M. Kato, and K. Kataoka, *Selective Synthesis of Heterobifunctional Poly(ethylene glycol) Derivatives Containing Both Mercapto and Acetal Terminals.* Bioconjugate Chemistry, 2000. **11**: p. 947-950.

54. R. G. Shimmin, A.B.S., and P. V. Braun, *Polymer Size and Concentration Effects on the Size of Gold Nanoparticles Capped by Polymeric Thiols.* Langmuir, 2004. **20**: p. 5613-5620.

55. E. Oh, K.S., R. Goswami, and H.Mattoussi, *One-Phase Synthesis of Water-Soluble Gold Nanoparticles with Control over Size and Surface Functionalities.* Langmuir, 2010. **26**(10): p. 7604–7613.

56. Sha, L., *Polyethylene glycol–coated (PEG5000) gold nanoparticles.* Molecular Imaging and Contrast Agent Database (MICAD), 2010: p. 1-4.

57. D. J. Lavrich, S.M.W., S. L. Bernasek, and G. Scoles, *Physisorption and Chemisorption of Alkanethiols and Alkyl Sulfides on Au(111).* Journal of Physical Chemistry, 1998. **102**: p. 3456-3465.

58. Cleland, W.W., *Dithiothreitol, a New Protective Reagent for SH Groups.* Biochemistry, 1964. **3**(4): p. 480-482.

59. F. Zhang, M.W.A.S., R. M. J. Jacobs, S. Zorn, R. A. Martin, C. M. Martin, G. F. Clark, G. Goerigk, and F. Schreiber, *Gold Nanoparticles Decorated with Oligo(ethylene glycol) Thiols: Protein Resistance and Colloidal Stability.* Journal of Physical Chemistry, 2007. **111**: p. 12229-12237.

60. M. Zheng, F.D., and X. Huang, *Ethylene Glycol Monolayer Protected Nanoparticles for Eliminating Nonspecific Binding with Biological Molecules.* Journal of American Chemical Society, 2003. **125**: p. 7790-7791.

61. N. W. S. Kam, M.O.C., J. A. Wisdom, and H. Dai, *Carbon nanotubes as multifunctional biological transporters and near-infrared agents for selective cancer cell destruction.* Proceedings of the National Academy of Sciences, 2005. **102**(33): p. 11600 –1160.

62. Chothia, C., *The Molecular Structure of Cell Adhesion Molecules.* Annual Review Biochemistry, 1997. **66**: p. 823-862.

63. J. S. Desgrosellier, D.A.C., *Integrins in cancer: biological implications and therapeutic opportunities.* Nature Reviews, 2010. **10**: p. 9-22.

64. S. Chatterjee, A.M., J. Schradermeier and G. Y. Gillespie, *Human malignant glioma therapy using anti-AvB3 integrin agents.* Journal of Neuro-Oncology, 2000. **46**: p. 135–144.

65. J. S. Wadia, S.F.D., *Protein transduction technology.* Current Opinion in Biotechnology, 2002. **13**(1): p. 52-56.

66. J. P. Richard, K.M., H. Brooks, P. Prevot, B. Lebleu, and L. V. Chernomordik, *Cellular Uptake of Unconjugated TAT Peptide Involves Clathrindependent Endocytosis and Heparan Sulfate Receptors.* Journal of Biological Chemistry, 2005. **280**(15): p. 15300–15306.

67. A. Ferrari, V.P., C. Arcangeli, A. Fittipaldi, M. Giacca, and F. Beltram, *Caveolae-Mediated Internalization of Extracellular HIV-1 Tat Fusion Proteins Visualized in Real Time.* Molecular Therapy, 2003. **2**(8): p. 284-294.

68. C. C. Berry, J.M.d.l.F., M. Mullin, S. Wai Ling Chu, and A. S. G. Curtis, *Nuclear Localization of HIV-1 Tat Functionalized Gold Nanoparticles.* IEEE Transactions on Nanobioscience, 2007. **6**(4): p. 262-269.

69. H. Xie, A.G.T., W. R. Glomm, J. A. Ryan, M. K. Brennaman, J. M. Papanikolas, S. Franzen, and D. L. Feldheim, *Critical Flocculation Concentrations, Binding Isotherms, and Ligand Exchange Properties of Peptide-Modified Gold Nanoparticles Studied by UV-Visible, Fluorescence, and Time-Correlated Single Photon Counting Spectroscopies.* Analytical Chemistry, 2003. **75**(21): p. 5797-5805.

70. Y. Liu, M.K.S., J. Ryan, E. D. Kaufman, S. Franzen, and D. L. Feldheim, *Synthesis, Stability, and Cellular Internalization of Gold Nanoparticles Containing Mixed Peptide-Poly(ethylene glycol) Monolayers.* Analytical Chemistry, 2007. **79**: p. 2221-2229.

71. R. Bjerkness, C.-F.B., *Phagocyte C3-Mediated Attachment and Internalization: Flow Cytometric Studies Using a Fluorescence Quenching Technique.* Blut, 1984. **49**: p. 315-323.

72. Schmaljohann, D., *Thermo- and pH-responsive polymers in drug delivery.* Advanced Drug Delivery Reviews, 2006. **58**: p. 1655-1670.